Redox conditions and trace metal cycling in coastal sediments from the maritime Antarctic

Patrick Monien [a,1,*], Karsten Alexander Lettmann [a], Donata Monien [a], Sanja Asendorf [a], Anne-Cathrin Wölfl [b], Chai Heng Lim [a], Janis Thal [c], Bernhard Schnetger [a], Hans-Jürgen Brumsack [a]

[a] Institute for Chemistry and Biology of the Marine Environment (ICBM), Carl-von-Ossietzky Straße 9-11, 26129 Oldenburg, Germany.

[b] Alfred Wegener Institute for Polar and Marine Research, Wadden Sea Research Station, Hafenstrasse 43, 25992 List, Germany.

[c] University of Bremen, Department of Geosciences, Klagenfurter Straße, 28359 Bremen, Germany

*Corresponding author

[1] Present address: University of Bremen, Department of Geosciences, Klagenfurter Straße, 28359 Bremen, Germany

E-mail addresses: monien@icbm.de (P. Monien), lettmann@icbm.de (K. A. Lettmann), donata.monien@icbm.de (D. Monien), sanja.asendorf@gmx.de (S. Asendorf), anne-cathrin.woelfl@awi.de (A.-C. Wölfl), chaiheng753@yahoo.com (C. H. Lim), ja_th@uni-bremen.de, schnetger@icbm.de (B. Schnetger), brumsack@icbm.de (H.-J. Brumsack)

Keywords: Antarctic coastal sediments, pore waters, early diagenesis, sulphate reduction, iron fertilisation

Abstract

Redox-sensitive trace metals (Mn, Fe, U, Mo, Re), nutrients and terminal metabolic products (NO_3^-, NH_4^+, PO_4^{3-}, total alkalinity) were for the first time investigated in pore waters of Antarctic coastal sediments. The results of this study reveal a high spatial variability in redox conditions in surface sediments from Potter Cove, King George Island, western Antarctic Peninsula. Particularly in the shallower areas of the bay the significant correlation between sulphate depletion and total alkalinity, the inorganic product of terminal metabolism, indicates sulphate reduction to be the major pathway of organic matter mineralisation. In contrast, dissimilatory metal oxide reduction seems to be prevailing in the newly ice-free areas and the deeper troughs, where concentrations of dissolved iron of up to 700 µM were found. We suggest that the increased accumulation of fine-grained material with high amounts of reducible metal oxides in combination with the reduced availability of metabolisable organic matter and enhanced physical and biological disturbance by bottom water currents, ice scouring and burrowing organisms favours metal oxide reduction over sulphate reduction in these areas. Based on modelled iron fluxes we calculate the contribution of the Antarctic shelf to the pool of potentially bioavailable iron (Fe_b) to be 6.9×10^3 to 790×10^3 t yr^{-1}. Consequently, these shelf sediments would provide an Fe_b flux of 0.35–39.5 mg m^{-2} yr^{-1} (median: 3.8 mg m^{-2} yr^{-1}) to the Southern Ocean. This contribution is in the same order of magnitude as the flux provided by icebergs and significantly higher than the input by aeolian dust. For this reason suboxic shelf sediments form a key source of iron for the high nutrient-low chlorophyll (HNLC) areas of the Southern Ocean. This source may become even more important in the future due to rising temperatures at the WAP accompanied by enhanced glacier retreat and the accumulation of melt water derived iron-rich material on the shelf.

1. INTRODUCTION

The microbially mediated mineralisation of organic material forms a major process controlling redox conditions and therefore the cycling of trace metals and nutrients in marine sediments (e.g., Elderfield et al., 1985; Shaw et al., 1990). Since the oxidation of carbon is coupled to the reactivity and availability of electron acceptors, like O_2, nitrate, Mn(IV), Fe(III) or sulphate, their occurrence or absence in pore waters provides valuable information on redox conditions in the sediment (e.g., Beck et al., 2008b; Canfield and Thamdrup, 2009). Redox-sensitive trace metals (Fe, Mn, V, Mo, U, Re) and nutrients (NO_3^-, NO_2^-, NH_4^+, PO_4^{3-}) have therefore been successfully used to decipher the redox state and biogeochemical processes in a wide range of coastal marine and deep-sea sediments of the North Atlantic, the North Pacific, the North Sea and off Peru (Froelich et al., 1979; Shaw et al., 1990; Canfield et al., 1993; Morford et al., 2005; Beck et al., 2008b; Beck et al., 2008a; Scholz et al., 2011; Morford et al., 2012). Several studies have shown that in the neritic zone, where the aerobic layer is often only a few millimetres thick, sulphate reduction is considered to be the dominant pathway of anaerobic organic matter degradation, which accounts for up to 92% of carbon oxidation (Jørgensen, 1982; Thamdrup and Canfield, 1996; Kostka et al., 1999). In areas with Mn and Fe-rich surface sediments metal oxide reduction may play a major role as well (Canfield et al., 1993; Thamdrup and Canfield, 1996; Rysgaard et al., 1998; Vandieken et al., 2006).

To date there are only a few studies dealing with geochemical processes and organic matter degradation in coastal marine sediments in the sub-Antarctic or Antarctic. Hartnett et al. (2008), for example, calculated benthic oxygen fluxes and denitrification rates from pore water profiles collected close to Anvers Island at the western Antarctic Peninsula. They could show that O_2 consumption rates on the Antarctic continental margin are comparable to rates found in other typical continental margin sediments. The influence of bioturbation on nutrient (NH_4^+, NO_3^-) exchange rates across the sediment-water interface were analysed in sediments from Factory Cove, Signey Island, South Orkney Islands by Nedwell and Walker (1995). Further studies dealt with sulphate reduction rates in Subantarctic sediments off

Signey Island (Nedwell, 1989) and in Ellis Fjord, Vestfold Hills, East Antarctica (Franzmann et al., 1988). However, investigations about early diagenetic processes and the behaviour of redox-sensitive trace elements in Antarctic pore waters are rare and restricted to deep sea regions of the Southern Ocean (e.g., King et al., 2000). This gap is astonishing as the Southern Ocean is known to be a high nutrient-low chlorophyll (HNLC) region where primary production is limited by the availability of bioavailable iron (e.g., Martin et al., 1990; Boyd et al., 2007). Consequently, the recycling of trace metals in Antarctic shelf sediments and their subsequent release into the water column could possibly represent an important source of bioavailable iron to the Southern Ocean, as it has been proposed by a number of authors (Planquette et al., 2007; Dulaiova et al., 2009; Lancelot et al., 2009; Tagliabue et al., 2010; Shaw et al., 2011; de Jong et al., 2012; Measures et al., 2012; Raiswell and Canfield, 2012 and references therein; Hatta et al., 2013; Measures et al., 2013).

In this study we for the first time report data on redox-sensitive trace metals (Mn, Fe, Mo, U, Re), nutrients (NO_3^-, PO_4^{3-}), sulphate and terminal metabolic products (NH_4^+, H_2S, total alkalinity) determined in pore waters from Potter Cove, King George Island, maritime Antarctica. In combination with solid-phase data (bulk parameters, like TOC and TS) we intend to shed light on controlling factors of early diagenetic processes and redox conditions at different locations in this model area. Moreover, based on a modelling approach, the potential of Antarctic shelf sediments as a significant source of bioavailable iron for the Southern Ocean will be discussed.

2. GEOCHEMICAL BACKGROUND

2.1 Trace element geochemistry

2.1.1 Iron

In oxic environments sediment iron is naturally occuring as solid Fe(II) and Fe(III) bearing silicates and (hydr)oxides (Poulton and Raiswell, 2005; Schroth et al., 2009). During early diagenetic processes in the sediment microbially mediated reduction and dissolution of reactive Fe (oxyhydr)oxides can occur leading to an enrichment of dissolved Fe(II) in the pore water (e.g., Canfield et al., 1993). Whereas in the presence of H_2S Fe (hydr)oxides (e.g., ferrihydrite or lepidocrocite) rapidly react to insoluble Fe(II) phases, like FeS and finally pyrite (FeS_2), residual Fe silicates require more than a century for a significant sulphidisation due to their slower reaction kinetics (Canfield, 1989; Canfield et al., 1992; Raiswell and Canfield, 1996).

2.1.2 Manganese

While stable in its oxidised and solid form in oxic seawater, Mn(IV) oxides are reduced to dissolved Mn(II) (and Mn(III)) in suboxic sediments (Stumm and Morgan, 1981; Trouwborst et al., 2006; Madison et al., 2013). With increasing alkalinity production in deeper, anoxic sediment layers Mn(II) is fixed again to the sediments by precipitation of mixed Ca–Mn carbonates (Middleburg et al., 1987; Jakobsen and Postma, 1989; Mucci, 2004). Mn (hydr)oxides are associated with Fe and some trace elements (e.g., As, Co, Mo, Ni, V) which are either incorporated or adsorbed on their surface and whose cycling is directly linked to dissolution and precipitation processes of the respective (hydr)oxide (e.g., Shaw et al., 1990; Burdige, 1993).

2.1.3 Rhenium

Rhenium is characterised by its conservative behaviour in marine waters, presumably present as an oxyanion ($Re(VII)O_4^-$) at 39.8 ± 0.2 pM (corrected to 35‰ salinity; Anbar et al., 1992; Colodner et al., 1995). In suboxic pore water ReO_4^- is probably reduced to Re(IV) and

presumably precipitated as ReS_4 into sediments where conducive conditions for organic matter oxidation by Fe(III) and sulphate reduction are persisting (Colodner et al., 1993; Morford et al., 2012).

2.1.4 Molybdenum

Being generally conservative in oxic marine environments, molybdenum is present as dissolved molybdate ($Mo(IV)O_4^{2-}$) showing concentrations of around 110 nM at a salinity of 35‰ (Morris, 1975; Algeo and Tribovillard, 2009). However, under certain conditions a temporary non-conservative behaviour of molybdenum, which may be fixed by transparent exopolymer particles (TEP) in aggregrates during the breakdown of plankton blooms is possible as well (Dellwig et al., 2007). In reducing sediments when hydrogen sulphide concentrations in the pore water exceed 50–250 µM (Helz et al., 1996; Zheng et al., 2000) MoO_4^{2-} is subsequently transformed into dissolved thiomolybdates ($MoO_xS_{4-x}^{2-}$, x = 0 to 3) and finally scavenged as particle-reactive tetrathiomolybdate (MoS_4^{2-}) by iron sulphides and/or humic materials (Bertine and Turekian, 1973; Erickson and Helz, 2000; Tribovillard et al., 2004; Vorlicek et al., 2004). Furthermore, pore water geochemistry of Mo is strongly linked to the cycling of Mn and Fe due to the fact that Mo adsorbs onto iron and manganese (oxy)hydroxides and is released during their reductive dissolution at or below the sediment-water interface (Crusius et al., 1996; Helz et al., 1996).

2.1.5 Uranium

Uranium shows a conservative behaviour in oxygenated seawater where it is present as soluble U(VI) carbonate complex ($UO_2(CO_3)_3^{4-}$) at approximately 13 nM (Ku et al., 1977; Langmuir, 1978). According to Klinkhammer & Palmer (1991) 75% of the removal of dissolved U from the ocean is related to the diffusion of U into suboxic sediments. Below the iron reduction zone and mediated by bacterial Fe and sulphate reduction it is reduced to U(IV) or U(III) and finally deposited as stable UO_2 (Lovley et al., 1991; Sani et al., 2004). Several studies moreover underline the evident association between U and Fe oxides, which

157 seem to co-cycle in suboxic sediments (Barnes and Cochran, 1990; Church et al., 1996; Duff
158 et al., 2002; Morford et al., 2007).
159
160 **3. REGIONAL SETTING**
161 Potter Cove is a 4 km long and 2.5 km wide tributary inlet at the southwestern end of King
162 George Island (KGI, 62°23'S, 58°27'W), the largest of the South Shetland Islands (Fig. 1). A
163 shallow (<30 m) transversal sill separates the inner (~3.0 km^2) from the outer cove
164 (~3.5 km^2), which is characterised by a broad intertidal area with water depths between 100
165 and 200 m in the southeast and extensive underwater macroalgal forests on hard bottom at
166 its coasts (Klöser et al., 1994; Iken et al., 1998). In the inner cove, in contrast, where water
167 depths do not exceed 50 m, soft substrate is dominant. While Fourcade Glacier has covered
168 half of the inner cove in the 1950s, its tidewater front has been retreating more than 1 km to
169 the east and is grounding on the shore since c. 2008 (Rückamp et al., 2011). Nowadays,
170 high glacial cliffs grounded on bedrock surround the cove in the northern and eastern sector,
171 whereas a broad sandy beach delimits the bay in the south. Between July/August and
172 October Potter Cove is completely covered by ice, which starts to break up end of
173 October/early November (Yoon et al., 2004). During the rest of the year the cove is ice-free
174 and the hydrology of Potter Cove is dominated by saline and cold subsurface waters (34.0–
175 34.5 psu, <0°C) from the adjacent Maxwell Bay, which enters the cove in the northwestern
176 part in a generally wind-driven cyclonic circulation pattern (Roese and Drabble, 1998). It is
177 overlain by a surface layer of less saline and warmer water (<34 psu, 0–1°C) influenced by
178 seasonally and interannually varying freshwater discharge from the melting Fourcade glacier
179 and surface runoff (Khim and Yoon, 2003). Three main streams with different regimes
180 (snowy-lacustrine in the southwest and snowy-glacial in the south-east) carrying sediment-
181 laden melt water meander through the southern shore. By these streams about 0.14 kg m^{-3}
182 of fine-grained suspended particulate material (0.0042–0.532 kg s^{-1}) is transported into
183 coastal waters during the melting period (Schloss et al., 2002).
184

185 **4. MATERIAL & METHODS**

186 **4.1 Sampling**

187 During austral summers 2009/2010 and 2010/2011 46 sediment cores, characterised by an
188 overlying water column showing no evidence for resuspended sediment and a clearly defined
189 sediment-water interface were retrieved in Potter Cove, King George Island (Fig. 1).
190 Sampling was done using a modified sediment corer (UWITEC, Austria) with an additional
191 weight of 12 kg (GC) and push corers (PC) operated by the Argentine Diving Division, with a
192 diameter of 5.7 and 5.4 cm, respectively. Moreover, five surface sediment samples were
193 taken at locations where coring was not possible using a Van Veen grabber (Fig. 1). Directly
194 after core recovery sediment cores were transported in upright position to the field lab
195 avoiding any kind of vibration. 13 of these cores were immediately sampled for pore waters
196 in 1- (0–5 cm), 2- (7–27 cm) and 5-cm resolution (≥30 cm). Therefore ultrapure water-
197 washed rhizons (0.15 µm mean pore size, Rhizosphere Research Products, The
198 Netherlands) were inserted simultaneously into the core liner through pre-drilled holes that
199 were covered by transparent adhesive tape and pore waters were collected in 12 mL
200 syringes. One aliquot of each pore water sample was filled in 5 mL polypropylene (PP) tubes
201 (conditioned with 2% HNO_3 conc. (subboiled)), acidified with nitric acid (≥69%, TraceSelect®,
202 Sigma Aldrich, Germany) to pH <2, stored at 4°C and transported to the home lab for major
203 and trace element analyses (Na, S, P, Fe, Mn, Mo, Re, U). A second aliquot was directly
204 measured for nutrients and total alkalinity (TA) at Carlini station within one hour after core
205 sampling. For selected cores (P02–P08) a third aliquot of 1.5 mL was directly given in a 2 mL
206 PP tube (Eppendorf, Germany) already filled with 0.6 mL of a 50 mM Zn acetate solution for
207 H_2S analysis. Sediments of parallel cores were sampled at 1-cm resolution, filled in pre-
208 weighed polyethylene (PE) bags, weighed, lyophilised and weighed again to calculate the
209 water content of each sample. Where no parallel cores could be recovered (K17, K23, K48,
210 KX1, KX4, P03) sediment samples were taken directly after the cores have been sampled for
211 pore water following the procedures described above. Original depths of sediment samples
212 were then estimated by using a correction factor (core length before pore water sampling

213 divided by the core length after pore water sampling) to account for the loss in core length
214 during pore water sampling.
215
216 **4.2 Pore water analyses**
217 Nutrients (NO_2^-, NO_x^-, NH_4^+) and TA were measured on pore water samples directly on-site
218 with a Multiscan GO microplate spectrophotometer (Thermo Fisher Scientific, Finland)
219 following the procedures after Miranda et al. (2001), Schnetger and Lehners (2014), Benesch
220 and Mangelsdorf (1972) and Sarazin et al. (1999) with slight modifications. Whereas
221 ammonia analyses were done on $HgCl_2$ poisoned samples (Kattner, 1999) two weeks after
222 pore water sampling, all other parameters where determined within 1 h of sampling on non-
223 poisoned sample aliquots. Nitrate (NO_3^-) was calculated from the difference between NO_x^-
224 and NO_2^-. H_2S was analysed following the method described by Cline (1969), which was
225 adapted to microtiter plate wells. Major and trace elements (Na, Fe, Mn, SO_4^{2-} (as total
226 sulphur), PO_4^{3-} (as total phosphorus)) were determined after a 2-fold dilution by inductively
227 coupled plasma optical emission spectroscopy (iCAP 6000, Thermo Scientific, Germany)
228 using a spiked seawater standard for calibration and several internal standards for matrix
229 correction (see Beck et al., 2008b for further information). Further, trace element analyses
230 (Fe, Mn, Mo, Re, U) of 20-fold diluted sample aliquots were performed using an Element 2
231 inductively coupled plasma mass spectrometer (Thermo Scientific, Germany) following the
232 procedure of Rodushkin (1998). Since we cannot exclude that nanoparticulate and colloidal
233 Fe might have even passed the 0.15 µm filter of the rhizons used in this study, it should be
234 noted here that the resulting Fe concentrations may represent a mixture of truly dissolved Fe
235 (operationally defined as passing through a 0.02 µm filter; see Raiswell and Canfield, 2012)
236 as well as nanoparticulate (<0.1 µm) and colloidal species (<1 µm).
237
238 **4.3 Sediment analyses**
239 Total sulphur (TS) and total carbon (TC) on sediment core samples were analysed on fine-
240 ground samples (<0.125 mm in agate ball mills) by means of a CS analyser (ELTRA CS 500,

Germany) equipped with a solid-state infrared detector. The content of total inorganic carbon (TIC) was determined coulometrically using a CM 5012 CO_2 coulometer coupled to a CM 5130 acidification module (UIC, Joliet, USA) whereas total organic carbon (TOC) was then calculated as the difference between TC and TIC (Babu et al., 1999). Based on the pore water salinity a correction for sea salt was carried out for all element concentrations. Where no pore water data were available sulphate concentrations were estimated using conventional seawater composition and a salinity of 34 psu.

4.4 Calculation of sulphate depletion

The depletion in sulphate ($SO_4^{2-}{}_{dep}$) representing the net amount of sulphate consumption via microbial SO_4^{2-} reduction was determined for each sediment depth using the following formula modified after Weston et al. (2006):

$$SO_{4dep}^{2-} = \left(\frac{Na_{PW}^{+}}{MR_{SW}}\right) - SO_{4PW}^{2-} \quad (1)$$

where $Na^{+}{}_{PW}$ and $SO_4^{2-}{}_{PW}$ are the measured molar concentrations of sodium and sulphate in the pore water and MR_{SW} is the molar ratio of Na^{+} and SO_4^{2-} which is assumed to be constant in oxic surface seawater (MR = 16.6). Since the ratio of $Na^{+}{}_{PW}$ to MR_{SW} represents the `expected´ SO_4^{2-} concentration in the pore water with a given salinity, the difference between this concentration and $SO_4^{2-}{}_{PW}$ is consequently an estimate for the metabolic amount of sulphate reduction which is concomitantly corrected for slight changes in salinity due to fresh water input (e.g., atmospheric-, melt-, and ground water).

4.5 Estimation of sulphate and iron reduction rates and fluxes

Sulphate (SRR) and iron reduction rates (FeRR) (FeRR are not shown) of selected cores were estimated using the REC (Rate Estimation from Concentrations) model after Lettmann et al. (2012). This numerical procedure is based on the 1-D steady state diagenetic transport reaction equation for dissolved compounds, which is inverted by Tikhonov regularisation, a

common and robust technique for solving ill-conditioned inverse problems (Lettmann et al., 2012). In addition to the determined sulphate and iron concentrations in the pore water, a few other parameters were needed for reduction rate calculation using the REC model. The effective diffusion coefficients in the pore water volume of the sediment (D_{Sed}) were calculated after Boudreau (1997) following equation 2:

$$D_{sed} = \frac{D}{\theta^2} \quad (2)$$

where D represents the respective molecular diffusion coefficient of sulphate (0.04662 $m^2\ s^{-1}$; Boudreau, 1997) and iron (0.03162 $m^2\ s^{-1}$; Boudreau, 1997) in the seawater at 0°C, 34 psu and 3 atm and Θ is the tortuosity. According to Boudreau (1997) the tortuosity can be estimated from the porosity Φ by:

$$\Theta = \sqrt{1 - ln(\Phi^2)} \quad (3)$$

where Φ of each sediment layer was calculated using the following equation:

$$\Phi = \frac{m_w - m_d}{V \cdot \rho_{SW}} \quad (4)$$

where V is the volume (in cm^3), m_w is the wet weight (in g) and m_d is the dry weight (in g) of each sample and ρ_{sw} is the density of seawater (in g cm^{-3}). Moreover, bioturbation was considered in this model by using the bioturbation coefficient D_b, which was calculated after Tromp et al. (1995):

$$log_{10}(D_b) = 1.63 - 0.05 \cdot log_{10}\omega \quad (5)$$

assuming an average regional sedimentation rate of ω = 0.3 cm yr^{-1} during the last century (0.04–1.7 cm yr^{-1}, average: 0.3 cm yr^{-1}; Monien et al., 2011; Majewski et al., 2012).

Finally, total fluxes of Fe (F_T) across the sediment-water interface were calculated for each location based on the advective flux and the total diffusive flux according to equation 6:

$$F_T = F_D + F_A \quad (6)$$

Here, the advective flux F_A was calculated with the sedimentation rate (burial rate), pore water porosity and the top-most measured pore water concentration value C_0:

$$F_A = \Phi \omega C_0 \quad (7)$$

The diffusive flux F_D, in contrast, represents the sum of the molecular diffusive part and the bioturbative part:

$$F_D = -\Phi(D + D_b)\frac{dC}{dz} \quad (8)$$

with $\frac{dC}{dz}$ denoting the estimated first derivative of the fitted pore water concentration profile obtained from the REC model at the top most sample location. This procedure of calculating the total flux F_T across the sediment-water interface by using the REC model results can be considered as appropriate as the data sampling intervals close to the sediment-water interface were sufficiently small to capture and resolve the local chemical processes.

4.6 Statistics

For validation of the methods carefully selected international and in-house (in italic) reference materials were measured for sediment (*Loess, Peru-1, UT-S*) and pore water analyses (NASS-5, CASS-5 (both NRC, Canada), spiked Atlantic Seawater (Osil, UK), single-element

standard solutions (Alfa Aesar, U.S.)). The pooled relative standard deviation (RSD_{pooled}) after Skoog & Leary (1996) was used to determine the degree of statistical spread and therefore the precision of a method. To get an idea of the accuracy of a method the relative error *f* representing the variation from the certified value is determined (Skoog and Leary, 1996). The results of the statistical evaluation are given in Table 2. The precision of sediment analyses (TS, TC, TIC) was ≤5% and accuracy ranged from -0.6 to 2.5% (TOC: -1.2%). In case of pore water analyses precision was better than 5% except for Re (7.5%) and very low (<0.03 µM) Mn (17%) and Fe (36%) concentrations. Generally accuracy ranged between -5.3% and 5.7% with only Re showing a higher relative error (11%). Where $|f|$ >5% (major elements) and $|f|$ >10% (trace elements) correction factors were calculated based on one of the reference samples using other reference samples for validation in order to minimise systematic errors.

5. RESULTS & DISCUSSION

5.1 Core descriptions

In general, surface sediments from Potter Cove are dominated by homogenous brown-greyish silty-clays intermingled with ice-rafted debris. Worms and worm tubes found in all cores suggest a moderate to high bioturbation in these sediments. Whereas close to the glacier front (P04) more blackish coloured sediments revealing a possible sulphate reduction and the formation of iron sulphides are not found above 30 cmbsf, in the deeper areas of the cove first black spots and stripes are occurring between 10 cmbsf (P08) and 16 cmbsf (P05). In contrast, sampling locations near the southern coast are characterised by black, sulphidic sediments with a typical H_2S smell already present at 7–10 cmbsf (e.g., P07).

5.2 Pore water profiles and redox zonation of Potter Cove surface sediments

The pore water geochemistry of selected cores will be discussed on a site-to-site basis in order to get a general picture of redox conditions in three different zones in the studied bay. Locations include: a) the newly ice-free area close to the tidewater front at the northeast of

Potter Cove (P04), b) the deeper (>40 m water depth) troughs in the central part of the bay (P05, P08) and c) a shallower zone influenced by melt water discharge at the southern coast (K48, P07). We explicitly do not use major and trace element data of the solid phase for identifying early diagenetic processes as resulting enrichments or depletions in the sediments would be completely masked by the high sedimentation rate in this region (0.04–1.7 cm yr^{-1}, average: 0.3 cm yr^{-1}; Monien et al., 2011; Majewski et al., 2012).

5.2.1 Inner cove close to the tidewater glacier front

At site P04, which is located close to the glacier front in the northeastern section of Potter Cove pore water profiles of redox-sensitive nutrients and trace metals indicate the typical sequence of redox reactions in hemipelagic sediments as proposed by Froelich et al. (1979) and Canfield & Thamdrup (2009). As shown in figure 2 nitrate concentrations moderately decrease from bottom water concentrations (c. 25 µM) close to zero within the first 10 centimeters indicating subsequent denitrification under reducing conditions. Concurrently, Mn and Fe concentrations are steadily increasing in this core until 25 and 20 cmbsf before particularly Fe shows a steep decline towards the bottom of the core (Fig. 2). Generally, the broad ferruginous and manganous zones present in the upper 30 cm of core P04 with high concentrations of dissolved Fe (>300 µM) and Mn (177 µM) document the 'suboxic' character of these sediments. This is in line with measured concentrations of terminal metabolic products of organic matter degradation, such as total alkalinity (TA), ammonia and phosphate. A steady but rather slow increase in alkalinity with depth (8.9 mM at 30 cmbsf) and relatively low phosphate (<60 µM) and ammonia concentrations (<0.37 mM) suggest moderate microbial activity and recycling of nutrients in these sediments (Fig. 2). Although no evidence for a significant depletion in sulphate was found (Fig. 2) and although no smell of H_2S could be detected, it is likely that the removal of dissolved Fe from the pore water at the base of core P04 (>25 cmbsf) gives first evidence for the abiotic reduction of iron oxides by sulphide (Canfield and Thamdrup, 2009). The behaviour of other redox-sensitive transition metals even suggests an earlier onset of sulphate reduction at this location. Uranium, for

379 instance, shows an exponential decrease from bottom water concentration (c. 12 nM) at the
380 core top to near zero values at 15 cmbsf. Lovley et al. (1991) reported that microbial
381 reduction of U(IV) is associated with Fe(III)-reducing microorganisms, which supports our
382 finding that subsequent removal of U from pore water and Fe reduction does occur at similar
383 depths in core P04. However, this is not true for Mo, which widely follows the profile of
384 dissolved U showing minimum pore water concentrations (<4 nM) at 30 cm depth (Fig. 2). It
385 is generally accepted that Mo removal from pore water and authigenic Mo enrichment in
386 sediments can only be explained by the presence of free H_2S (Helz et al., 1996; Zheng et al.,
387 2000; Morford et al., 2005; Morford et al., 2007). This, in turn, suggests an onset of sulphate
388 reduction already in the upper 10 cm of the core, though not supported by the $SO_4^{2-}{}_{dep}$ profile
389 (Fig. 2). A similar finding was made by King et al. (2000) who observed a significant
390 depletion in pore water Mo in sediments of the Atlantic sector of the Southern Ocean without
391 any evidence of sulphidic conditions. A final explanation for the unusual behaviour of Mo in
392 core P04 could not be found in the context of this study. In summary it can be stated that
393 pore waters of surface sediments close to the glacier front show evidence for 'suboxic'
394 conditions, which are dominated by microbial nitrate and metal (Fe, Mn) oxide reduction
395 processes.
396
397 *5.2.2 The central inner cove*
398 Pore waters of sediments taken in the deeper (36–42 m water depth) central part of the inner
399 cove (cores P05, P08) are characterised by a more condensed redox zonation compared to
400 the stations close to the glacier front (Fig. 3). At both locations, nitrate is consumed within the
401 first two cmbsf followed by a relatively sharply bounded zone of dissolved Fe enrichment in
402 these pore waters peaking at c. 2–5 cmbsf. This trend is to some extent parallelled by Mn,
403 which shows a slower decline with increasing sediment depth. With 514 µM (P08) and
404 685 µM (P05), respectively, the central stations exhibit the highest concentrations of
405 dissolved Fe found in Potter Cove sediments. The parallel decreases in Re, U, and Mo in
406 core P08, which are accompanied by a gradual and moderate increase in terminal

metabolism products, such as TA (6.5 mM), phosphate (116 µM) and NH_4^+ (0.35 mM) indicate microbially induced organic matter degradation and nutrient recycling under progressively reducing conditions (Fig. 3). At station P05 a significant decline in Mo and Re is only recognisable below c. 15–19 cmbsf, which widely coincides with the lower boundary of the iron reduction zone (Fig. 3). Like at station P08, TA, ammonia, and phosphate concentrations are moderately elevated in P05 pore waters with a phosphate maximum of 180 µM directly within the iron reduction zone. This peak value is probably associated with the dissolution of iron phosphate phases (Tribovillard et al., 2006). Although the removal of Fe and Mo from the liquid phase in deeper sediment layers at both locations strongly suggests the presence of sulphidic conditions, neither an H_2S odor nor a significant depletion in sulphate (c. 1–2 mM) could be detected (Fig. 3). In total, the overall picture in the central part of the cove is of a pore water influenced by nitrate and metal oxide reduction in the upper section and the onset of sulphidic conditions in deeper sediments (>10-20 cmbsf).

5.2.3 Inner cove close to the melt water stream outlets and Carlini Station

At the shallower southern coast of the cove pore water profiles show characteristic sequences of “compressed” redox zonation as expected for nearshore marine sediments. At station K48 located close to the Potter Creek melt water stream outlet the nitrate reduction zone is relatively narrow and is followed by enhanced concentrations of dissolved Mn and Fe reaching maxima of 33 and 189 µM in the first 10 cmbsf, respectively (Fig. 4). The concurrent decreases in Re, Mo, and U accompanied by a steady increase in $SO_4^{2-}{}_{dep}$ (5 mM) and TA (11 mM) towards the base of the core let suggest more severe reducing conditions in these sediments compared to the other sites. Particularly the removal of iron from the pore water in deeper, more blackish sediments (>11 cmbsf) seems to mark the beginning of the sulphidic zone, where dissolved iron is probably fixed as iron sulphide in the solid phase again. Even stronger anoxic conditions were found at station P07, which is situated in c. 5 m water depth in front of Carlini Station. Whereas nitrate is completely reduced and removed from the pore water system in the first centimetre, only marginal concentrations of dissolved iron (max.

21 µM) and manganese (max. 6.4 µM) were found in restricted reduction zones of the upper core (Fig. 4). The following gradual increase in $SO_4^{2-}{}_{dep}$ (7.4 mM) and the occurrence of free H_2S in black sediment strongly suggest sulphidic conditions in depths below 5 cm (Fig. 4). It should be noted that free H_2S could not be detected in any other core analysed in this study. The presence of anoxic conditions is moreover supported by the rapid and simultaneous removal of U, Re, and Mo from the pore water in the same depth interval (Fig. 4). Accompanied by the decline in sulphate synchronous increases in total alkalinity (13.5 mM), ammonia (1.3 mM) and phosphate (450 µM) were observed indicating rapid mineralisation of organic matter in P07 surface sediments (Fig. 4). In summary, pore water geochemistry reveals intensive degradation of organic material in sediments from the southern coast dominated by sulphate reduction and only minor influence by nitrate and metal oxide reduction.

5.3 Pore water stoichiometry and sulphate reduction rates

In order to identify the predominant organic matter mineralisation process in Potter Cove surface sediments at the different sampling locations regression analyses between $SO_4^{2-}{}_{dep}$ as an estimate for the metabolic amount of sulphate reduction and total alkalinity (TA) as a terminal metabolic product were conducted. Following the GEOSECS Choice of Takahashi et al. (1982) in a marine environment the definition of TA can be simplified to:

$$TA = [HCO_3^-] + 2[CO_3^{2-}] + [H_2BO_3^-] \quad (9)$$

which would make TA a suitable substitute for dissolved inorganic carbon (DIC). This is in line with Beck et al. (2008a) who could show that TA equals DIC in deep pore waters obtained from intertidal flat sediments at the NW German coast. According to equation 6, although particularly valid for living marine phytoplankton (Redfield et al., 1963; Sholkovitz, 1973), we would expect a DIC:$SO_4^{2-}{}_{dep}$ (TA:$SO_4^{2-}{}_{dep}$) ratio of 2 if the degradation of organic material is mainly linked to sulphate reduction.

$$(CH_2O)_{106}(NH_3)_{16}H_3PO_4 + 53SO_4^{2-} + 14H^+ \rightarrow 53H_2S + 16NH_4^+ + H_2PO_4 + 106HCO_3^- \quad (10)$$

Figure 5 reveals that sulphate depletion in Potter Cove pore waters is indeed positively correlated to total alkalinity in most of the cores located at the southeastern coast (KX4, K48, P03) and in the vicinity of the research station (P07, KX1, K23). At these sites the TA: $SO_4^{2-}{}_{dep}$ ratio, which is given by the slope of the respective regression analysis ranges between 1.6 and 2.3 and is quite close to the expected value of 2 according to the Redfield ratio (Fig. 5). The presence of sulphate reducing conditions in Potter Cove sediments is not surprising. Several studies could already show that sulphate reduction is one of the main processes of organic matter degradation in coastal sediments, where the oxygen surface layer is often only a few millimetres thick and where it accounts for 10–92% of TOC oxidation (Jørgensen, 1982; Thamdrup and Canfield, 1996; Kostka et al., 1999; Gribsholt and Kristensen, 2003). Interestingly, this is not only true for temperate regions, but was also found in permanently cold coastal sediments from Svalbard, Arctic (Kostka et al., 1999) or from Signey Island, Subantarctic (Nedwell, 1989). Although we could show that sulphate reduction may represent the major pathway of organic matter mineralisation in this part of the bay, estimated sulphate reduction rates (SRR) are generally low. Using the numerical REC (Rate Estimation from Concentrations) model after Lettmann et al. (2012) integrated SRR of 0.23-0.56 mol m^{-2} yr^{-1} were calculated for the upper 20 cm of cores KX4, K23, K48 and P07, which show the highest depletion in sulphate (Fig. 6). These rates are significantly lower than SRR estimated for other subpolar or temperate regions, like Factory Cove, Signey Island (2.5 mol m^{-2} yr^{-1}; Nedwell, 1989), or the Danish coast (0.95–5.5 mol m^{-2} yr^{-1}; Sørensen et al., 1979), but comparable to SRR found in sediments off Greenland (0.39 mol m^{-2} yr^{-1}; Rysgaard et al., 1996). Probably this is due to the fact that particularly in the shallower areas close to the coast sediments are affected by enhanced physical disturbance, for example, by iceberg scouring. The resulting intrusion of oxygenated seawater into deeper layers would inhibit sulphate reduction and lead to lower sulphate reduction rates at the surface.

In contrast, an entirely different picture is given for the cores that were taken in newly ice-free areas directly at the glacier front (P02, P01, P04) and in the deeper troughs (P05, P08) in the centre of the cove (>40 m) (Fig. 5). Here, correlations between sulphate depletion and TA are rather poor or even negative. Though redox-sensitive trace elements, like Mo may give evidence for sulphate reduction in some of these cores this process alone seems not to be responsible for increases in total alkalinity/DIC during organic matter degradation. At these locations alternative metabolic pathways, involving nitrate, manganese and iron reduction may be more important as it could also be shown for Arctic sediments northeast of Svalbard (Vandieken et al., 2006).

5.4 Spatial distribution of redox conditions in Potter Cove surface sediments

The spatial distribution of selected pore water and solid phase parameters shows a picture of diverse redox conditions at different sites in the study area (Fig. 7). There is evidence for a significant reduction of sulphate in Potter Cove surface sediments (0–20 cmbsf) as high sulphate depletion is only found along the southern coast of Potter Peninsula and in the northwestern area of the inner cove. It is accompanied by enhanced microbial activity, which is reflected by an increased total alkalinity in the pore water. The presence of sulphidic conditions is moreover supported by higher maximum concentrations in total sulphur in the solid phase of these sediments indicating the formation of iron sulphides, like FeS_x and pyrite (Howarth and Jørgensen, 1984). Maxima of up to 0.4% TS were present in the shallower (<30 m) southeastern area of the bay where no pore water data are available. Considering that sea salt correction of solid phase sulphur may even be overestimated by assuming seawater composition of the pore water, the solid phase data strongly suggest even more intense sulphidic conditions in surface sediments in this area.

In contrary, close to the glacier front and in the deeper troughs (>40 m) of the central cove concentrations of terminal products of metabolism, like TA and phosphate are generally lower and sulphate depletion does not exceed 4 mM (Fig. 7). On the other hand, these sediments are characterised by high concentrations of dissolved iron in the upper 19 cmbsf.

With average iron concentrations of >300 µM in the centre and at least >250 µM in the northeast of the cove metal oxide reduction seems to be prevailing in these areas as has been shown in section 5.2. Maximum values of dissolved iron found in Potter Cove surface sediments (c. 700 µM) are even significantly higher than in any other study conducted so far. Morford et al. (2009), for example, reported Fe concentrations in coastal pore waters from Buzzard Bay, Massachusetts (USA) of up to 500 µM. Lower Fe concentrations were found in surface sediments in the California Borderland (<200 µM; Shaw et al., 1990) and from the Skagerak, Denmark (c. 180 µM; Canfield et al., 1993). Even in high-Arctic coastal marine sediments from Young Sound, Northeast Greenland where iron reduction is considered to be a major pathway of organic matter degradation, concentrations of dissolved Fe in the pore water do not exceed 300 µM (Rysgaard et al., 1998).

5.5 Factors controlling redox conditions in Potter Cove sediments

There are several factors affecting redox conditions in (coastal) sediments, such as the oxygen concentrations in the overlying water column or the quantity and quality of organic matter supplied to the sediment (Beck et al., 2008b). But also the rate of sediment accumulation, the occurrence of sediment disturbance, either by burrowing organisms or physical re-working and the availability of respective electron acceptors may influence the biogeochemical processes in the sediment as well (e.g., Sholkovitz, 1973; Aller et al., 1986). In the following possible controlling factors for spatial differences in dominating organic matter mineralisation pathways and redox conditions in Potter Cove sediments are discussed.

5.5.1 Availability of substrate

The quantity of organic carbon, which is buried in the sediment, forms certainly one of the major controls on sedimentary redox processes. Jørgensen et al. (1982) could already show that metabolic rates, which are triggered by the amount of suitable substrate, are positively correlated to the level of reducing conditions. TOC concentrations in Potter Cove surface

sediments (av. 0.53 ± 0.30%) are relatively low even for siliceous muds and oozes from the Antarctic continental shelf and the Bransfield Basin (av. 1.2–1.5%; Dunbar et al., 1989; Barcena et al., 1998) but comparable to values found by Milliken et al. (2009) and Monien et al. (2011) in sediments from the nearby Maxwell Bay (av. 0.3–0.4%). Higher values are particularly present in the (north)western part of the cove (0.5–1.3%), whereas TOC concentrations are lower (<0.4%) or even near zero in the newly ice-free areas in the east close to the glacier front (Fig. 7). With average molar TOC/TN ratios close to the ratio expected for phytoplankton (c. 6.6; Redfield et al., 1963) and local macroalgae (5.8–11.7; Weykam et al., 1996), a predominantly marine source for the organic material in Potter Cove sediments (6.1 ± 1.5) is indicated. As this average ratio is significantly lower than TOC/TN values of local mosses (40 ± 19), lichens (114 ± 46), liverworts (55 ± 3), grasses (21 ± 4) or freshwater algae from the adjacent lakes (8.3 ± 1.4) (Lee et al., 2009), an appreciable input of terrestrial and therefore less digestible organic matter from the enclosing peninsulas can be excluded. However, although primary production is generally high in the neritic zones around Antarctica (Martin et al., 1990), this is not the case for Potter Cove and adjacent areas where summer chlorophyll *a* (chl *a*) concentrations are generally below 1 mg m^{-3} (Schloss et al., 2012). Schloss et al. (2002) argue that a combination of several physical conditions, including an unfavourable depth of turbulent vertical mixing and the shading of surface waters by melt water derived suspended particulate matter may be a possible reason for relatively low phytoplankton growth in Potter Cove during austral summer. Therefore, it is more probable that macroalgae may represent a relevant contributor to the sedimentary TOC pool as it has already been proposed by Quartino et al. (2008). This may be supported by the fact that higher TOC concentrations are particularly found in surface sediments that are located adjacent to the hard bottom dominated areas in the outer and the western part of the inner cove (Fig. 7). In these zones, which are already ice-free since at least c. 60 years (Rückamp et al., 2011), high abundances of macroalgae are found whereas the newly ice free areas close to the glacier front are still only sparsely settled (Quartino et al., 2013). However, a higher accumulation of glacigenous material close to the glacier front, which

would dilute the TOC content in the sediment has to be considered as well. In any case, the lack of metabolisable organic material in the surface sediments in the eastern coast close to the glacier may to some extent serve as an explanation for less reducing conditions present in the sediments in this area. However, it fails to clarify the dominance of metal oxide reduction processes in the deposits of the deeper troughs of the central cove (P05, P08). Interestingly, their TOC concentrations are comparable or even higher than those present in surface sediments along the southern coast (0.2–0.5% vs 0–0.3%; Fig. 7).

5.5.2 Availability and reactivity of electron acceptors

Another controlling factor may be the availability and reactivity of respective electron acceptors, which are closely linked to organic matter mineralisation. According to Froelich et al. (1979) and Canfield and Thamdrup (2009) aerobic respiration is followed by the reduction of nitrate, Mn(IV), Fe(III), sulphate and finally methanogenesis. Their order of utilisation is based on the thermodynamics of the processes and the energy available to the organisms; an overlap between some of these processes is also possible (Canfield and Thamdrup, 2009). Whereas sulphate is practically non-limiting in marine subsurface sediments due to its high concentration in seawater (Jørgensen, 1982), this is not necessarily true for reducible Fe phases. It is commonly accepted that only a fraction of the sedimentary iron is on the short-term available for microbially mediated iron reduction. Iron reactivity depends on factors, like mineralogy, crystallinity, and grain size (Postma, 1993 and references therein). Consequently, iron reduction will only dominate over sulphate reduction as long as the sediments still contain reactive iron (oxyhydr)oxide minerals, such as ferrihydrite, lepidocrocite, goethite and haematite, whose half-lives with respect to reductive dissolution and sulphidation range between some minutes to a couple of days (Canfield et al., 1992; Raiswell and Canfield, 1996; Poulton et al., 2004). However, when this pool of reactive metal oxides and iron (oxyhydr)oxides in particular is exhausted, as it is the case at some locations along the southern coast of the bay (P07), sulphate reduction is the predominant pathway of organic matter degradation. This is not only indicated by the lack of significant enrichments in

603 dissolved Mn and Fe, but also by the occurrence of free H_2S in the pore water, which is no
604 longer required for precipitating FeS_2 or its precursor FeS.
605 The situation is different in the central cove and close to the glacier front, where sulphate
606 depletion seems to be negligible and where moderate increases in terminal products of
607 metabolism (TA, PO_4^{3-}) are linked to high Mn and Fe concentrations. A similar phenomenon
608 was observed by Aller et al. (1986) who investigated muds from the inner Amazon shelf.
609 They related the presence of extensive iron reduction zones (>1 m), which showed no
610 evidence of significant sulphate depletion, to the periodical regeneration of the reactive Fe
611 pool by physical re-working. Particularly for shallower coastal Antarctic regions it is known
612 that anchor ice, iceberg scouring and water turbulence produced by tides and waves are
613 disturbance mechanisms affecting the surface sediments and the coastal biota (Arntz et al.,
614 1994). It is probable that these mechanisms are also responsible for physical re-working of
615 Potter Cove sediments although we would rather expect this for the shallower areas at the
616 southern coast. The occurrence of sediment resuspension events in Potter Cove during
617 times when strong eastern winds lead to a homogenisation of the water column was already
618 shown by Klöser et al. (1994). Preserved ice growlers and ice furrows evidencing the
619 occurrence of iceberg scouring could moreover be detected mainly in the central part of the
620 cove by side-scan sonar data (Pasotti et al., accepted manuscript). In addition, an enhanced
621 activity of burrowing organisms in well-bioturbated surface sediments has to be considered
622 as well.
623 A further and more likely possibility could be the increased deposition of reactive iron-rich
624 material at these locations. Every year during the summer months c. 3,000 t of fine-grained
625 suspended particulate matter (SPM) are transported into the cove by sediment laden melt
626 water streams on Potter Peninsula (D. Monien, personal communication). These calculations
627 do not include the subglacial input of SPM from underneath the Fourcade Glacier front,
628 which was estimated to be even higher (c. 24,000 t yr^{-1}; D. Monien, personal
629 communication). Granulometric analyses let assume that most of this fine-grained material is
630 deposited in the newly ice-free areas close to the glacier and in the deeper central cove (A.

631 Wölfl, personal communication). This is in line with an up-to-date current circulation model,
632 which shows that these deeper troughs possibly act as depocentres for this fine-grained
633 material (Lim, 2014). In addition, leaching experiments have shown that this SPM contains
634 appreciable amounts of dithionite leachable iron (FeD: 2.1–2.9%; D. Monien, personal
635 communication; Brünjes, 2013), which can potentially be reduced by microorganisms. This
636 FeD content is significantly higher than that found by other authors for iceberg-hosted
637 sediment in this area (FeD: 0.4–1.04%; Raiswell, 2011). The increased availability of reactive
638 iron is also reflected in the ratio of FeD and total iron in Potter Cove sediments (0.44 ± 0.04;
639 Brünjes, 2013; D. Monien, personal communication), which is higher than the compiled ratio
640 of 0.26 ± 0.09 found by Raiswell and Canfield (1998) for other continental margin, deep sea
641 and dysaerobic sediments. One possible explanation for this may be the enhanced Fe oxide
642 supply by pyrite oxidation. Dold et al. (2013), for instance, found evidence for acid rock
643 drainage (ARD) resulting from the microbially mediated oxidation of sulphide minerals in
644 nearby Cardozo and Marian coves. Although trace metal and pH/Eh data obtained from
645 superficial runoff on Potter Peninsula and from Potter Cove water column (D. Monien,
646 personal communications; Eraso and Dominguez, 2007) do not show any evidence for ARD
647 in the Potter Cove system, the infiltration of local pore waters by Fe^{2+}-rich groundwaters
648 cannot be completely ruled out.
649
650 **5.6 Coastal pore waters as a significant source of trace metals and micronutrients in**
651 **the Antarctic region**
652 Iron is considered to be an important micronutrient for marine primary producers (e.g., Martin
653 et al., 1990; Coale et al., 2004). Particularly in vast regions of the Southern Ocean iron limits
654 algae bloom development in this HNLC (high nutrient-low chlorophyll) area (Martin et al.,
655 1990; Lancelot et al., 2009). Therefore, the knowledge about contributors to the iron pool of
656 this system is of utmost importance. In addition to aeolian input, the contribution from acid
657 rock drainage and glacial flours, upwelling of replete deeper water masses, release of
658 terrigineous material from icebergs and iron-bearing subglacial streams, suboxic shelf

659 sediments are discussed to be a potential source of bioavailable iron (Fe_b) to the ocean
660 (Raiswell et al., 2006; Planquette et al., 2007; Raiswell et al., 2008; Dulaiova et al., 2009;
661 Tagliabue et al., 2010; Raiswell, 2011; Shaw et al., 2011; de Jong et al., 2012; Measures et
662 al., 2012; Raiswell and Canfield, 2012 and references therein; Dold et al., 2013; Hatta et al.,
663 2013; Measures et al., 2013; Hopwood et al., 2014). Only a small amount of microbially
664 reduced and remobilised Fe(II), which diffuses from the sediment into the oxic water column
665 will be stabilised by natural organic ligands as aqueous Fe(III) (Rue and Bruland, 1995), a
666 form that is principally bioavailable (Chen and Wang, 2001). Most of the iron will be rapidiy
667 re-oxidised to Fe(III) and due to its low solubility in oxic seawater precipitated as extremely
668 reactive nanoparticulate ferrihydrite (Raiswell and Anderson, 2005). These ferrihydrites are
669 to some extent scavenged by suspended material and re-deposited in the sediment, where
670 they can easily be reduced again. A certain amount may be kept in suspension and
671 transported for longer distances across the shelf (Lam et al., 2012). By vertical diffusion or
672 during upwelling events these reactive and labile iron phases may be delivered to the mixed
673 surface layer and represent a key source of bioavailable iron as could be shown by Lam and
674 Bishop (2008) for the HNLC western Subarctic Pacific. Using naturally occurring radium
675 isotopes as a tracer for shelf-derived components Dulaiova et al. (2009) could show that the
676 entrainment of iron-rich waters from the South Shetland Islands shelf into HNLC waters of
677 the southern Drake Passage seems to be an effective transport mechanism for this
678 biolimiting micronutrient. This is supported by more recent studies from this region, which
679 combined phytoplankton abundances, trace metal (Al, Fe, Mn) and transmissometer data of
680 surface waters (<500 m water depth) (Hatta et al., 2013; Measures et al., 2013). These
681 authors reported significant lateral fluxes of Fe from the Antarctic Peninsula shelf to the Fe
682 depleted ACC. Moreover, they concluded that the process of sediment resuspension as the
683 ACC water reaches the AP shelf and the concurrent release of diagenetically produced iron
684 from suboxic shelf sediments is the most likely iron source. This shelf-derived iron, in turn,
685 will be rapidly transported offshore by the local current system and may fuel extensive
686 phytoplankton blooms in areas downstream of the Ona Basin and the Scotia Sea (Hatta et

687 al., 2013; Measures et al., 2013; Zhou et al., 2013). However, while they could estimate the
688 iron supply into offshore waters of the southern Drake Passage, they were not able to
689 calculate Fe_b fluxes originating from the shelf due to the lack of pore water data.
690 Using the REC model after Lettmann et al. (2012) we were able to estimate Fe fluxes derived
691 from Potter Cove sediments ranging between c. 1.4 and 155 mmol m^{-2} yr^{-1} (median:
692 15 mmol m^{-2} yr^{-1}; Table 3). It is important to state here that this flux does not represent the
693 flux of truly dissolved Fe and may include a considerable contribution from acidified
694 nanoparticles, colloidals and iron bound by organic ligands. These iron species may,
695 however, be made bioavailable by photoreduction in the euphotic zone or by remineralisation
696 processes (Boyd and Ellwood, 2010). Recent studies even suggest a direct uptake of
697 colloidal and ligand-bound iron by certain phytoplankton species (Boyd and Ellwood, 2010
698 and references therein; Jiang et al., 2013). Nonetheless, we have to keep in mind that the
699 iron flux in this area may still be a conservative estimate for the average Fe flux from the
700 Antarctic shelf since iron reduction may play an even more significant role in deeper (c.
701 500 m) hemipelagic areas. Moreover, it should be noted that our model only assumes an iron
702 supply by diffusive fluxes neglecting the influence of physical sediment re-working (e.g. by
703 iceberg scouring and sediment resuspension), which may represent an important factor for
704 the release of dissolved iron from the sediment in this region (see chapter 5.5.2). Modelling
705 results based on a generic shelf sediment reveal that bioirrigation can account for up to 99%
706 of the total benthic recycling flux (Raiswell and Canfield, 2012).
707 In order to assess the significance of benthic recycling in Antarctic shelf sediments as a
708 source for bioavailable iron in the Southern Ocean some assumptions have to be made.
709 According to Elrod et al. (2004) the flux of recycled iron will be most efficiently transported to
710 surface waters to fuel primary production by upwelling at the eastern shelf margins. Since
711 these regions make up 5% of the global shelf area it may be reasonable to choose an export
712 efficiency of 5% for the shelf flux. This is still a very conservative assumption since it neglects
713 significant iron supply from more remote shelf areas by lateral transport, which recent studies
714 could show to be significant (Dulaiova et al., 2009; Hatta et al., 2013; Measures et al., 2013).

In addition, once the bioavailable iron has reached the upper water column we also have to account for a continuous vertical loss of iron by biological (removal by sinking faecal pellets and cell aggregates after ingestion by microorganisms) and abiotic processes (colloidal hydrolysis and subsequent scavenging by aggregation and adsorption onto sinking inorganic particles). By using Fe/Th ratios and $^{234}Th/^{238}U$ disequilibrium in offshore waters of the Elephant Island region (AP) Dulaiova et al. (2009) estimated that this vertical loss of dissolved Fe could amount to about 25%.

If we now consider that all Antarctic shelf areas with a maximum depth of 500 m (2.4×10^6 km^2; based on bathymetry data taken from Timmermann et al., 2010 and the grounding line position after Bindschadler et al., 2011) generate an iron flux comparable to the fluxes calculated for Potter Cove sediments and if we further consider that all Fe reaches the mixed surface layer with the export efficiency given above (5%) allowing for a vertical loss of nanoparticulate Fe in overlying seawater of 25%, the Antarctic shelf areas would contribute 6.9×10^3 to 790×10^3 tonnes per year to the pool of bioavailable iron (median: 77×10^3 t yr^{-1}). Consequently, these shelf sediments would provide an Fe_b flux of 0.35–39.5 mg m^{-2} yr^{-1} (median: 3.8 mg m^{-2} yr^{-1}) to the Southern Ocean (based on a total area of c. 20×10^6 km^2; Shaw et al., 2011). Even this presumed minimum flux is higher than the input by acid rock drainage (0.05 mg m^{-2} yr^{-1} Fe_b; Dold et al., 2013), aeolian dust (0.04–1 mg m^2 yr^{-1} Fe_b; Lancelot et al., 2009; Shaw et al., 2011; Raiswell and Canfield, 2012) and anoxic subglacial meltwaters (0.0055–5.5 mg m^{-2} yr^{-1} Fe_b; Wadham et al., 2013) (Table 4). Previous estimates of shelf-derived input of bioavailable iron range between 0.05 (Lancelot et al., 2009) and 0.64–1.6 mg m^{-2} yr^{-1} (Tagliabue et al., 2010) Fe_b and are therefore lower than our estimate if we consider the same export efficiency of 5% (Table 4). However, recent studies could show that these Fe_b fluxes that are based on ocean models or fluxes measured by Elrod et al. (2004) on the Californian Shelf might be underestimated. For their transect near Elephant Island, for example, Dulaiova et al. (2009) calculated a supply of dissolved iron of 2.3×10^3 t yr^{-1}. If this is scaled up for the whole bloom area north of the island (250 x 250 km), this would translate into a flux of 37 mg m^{-2} yr^{-1} (Dulaiova et al., 2009), which

743 is similar to our estimations (Table 4). The fact, that these fluxes are moreover comparable to
744 the contribution of iceberg–hosted material, which is assumed to be 2–20 mg m^{-2} yr^{-1} Fe_b
745 (Shaw et al., 2011) and 37.5–62.5 mg m^{-2} yr^{-1} Fe_b (Raiswell and Canfield, 2012) (Table 4)
746 makes Antarctic shelf sediments one of the major sources of bioavailable iron for the HNLC
747 regions of the Southern Ocean.
748
749 **6. CONCLUSIONS**
750 For the first time, redox-sensitive trace elements and nutrients are used to describe redox
751 conditions and biogeochemical processes in pore waters from coastal sediments at King
752 George Island, western Antarctic Peninsula. We could show that sulphate reduction is the
753 major pathway of organic matter mineralisation in the shallower areas at the southern coast
754 of Potter Peninsula and on a transect towards the northwestern area of the inner Potter
755 Cove. Sulphate reduction rates in the upper 20 cm of these sediments (0.23–0.56 mol m^{-2} yr^{-1})
756 are comparable to rates found in coastal sediments off Greenland but an order of
757 magnitude lower than known from nearshore deposits in other subantarctic or temperate
758 regions. In contrast, microbial manganese and dissimilatory iron reduction processes are
759 dominant in the deeper troughs of the central cove and in the newly ice-free area in glacial
760 proximity. We suggest that a combination of enhanced physical and biological disturbance by
761 bottom water currents, ice scouring and burrowing organisms, the increased accumulation of
762 melt water derived, fine-grained material with high amounts of reducible metal oxides and the
763 reduced availability of metabolisable organic matter favours metal oxide reduction over
764 sulphate reduction in these respective regions. Based on modelled iron fluxes we calculate
765 that the Antarctic shelf contributes 6.9 x 10^3 to 790 x 10^3 t yr^{-1} to the pool of bioavailable iron
766 (Feb), which would translate into an Fe_b flux of 0.35–39.5 mg m^{-2} yr^{-1} (median: 3.8 mg m^{-2} yr^{-1})
767 to the Southern Ocean. This contribution is presumed to be in the same order of
768 magnitude as the flux provided by icebergs and significantly higher than the input by aeolian
769 dust or previous estimates for the continental shelf. This makes the suboxic shelf sediments
770 a key source of iron for the HNLC areas of the Southern Ocean. As a consequence of

771 enhanced glacier retreat and melt water fluxes and the resulting rise of accumulation of iron-
772 rich sediment on the shelf (Monien et al., 2011; Majewski et al., 2012), it can be assumed
773 that the role of Antarctic shelf sediments for the natural iron fertilisation of the Southern
774 Ocean may even gain in importance in the future. This may particularly be true for the
775 contribution of sediments from shallow shelf areas, since increased melting may also
776 increase stratification, which in turn may cut off the Fe supply from deeper waters for broad
777 areas of the shelf making these shallow sediment sources even more important.
778

779 **ACKNOWLEDGEMENTS**

780 This study forms part of the IMCOAST project and was funded by the German Research
781 Foundation (DFG project no. BR 775/25-1) and the German Federal Ministry of Education
782 and Research (BMBF, ref. no. 03F0617C). We are grateful to the Argentine Diving Division
783 and the generous hospitality at Carlini Station during the field campaigns 2009/2010 and
784 2010/2011. Special thanks go to Oscar Gonzales (Instituto Antártico Argentino, Buenos
785 Aires) for the scientific coordination of the project during both field campaigns. Moreover, we
786 gratefully acknowledge the technical assistants at the ICBM (Institute for Chemistry and
787 Biology of the Marine Environment). Finally, we thank both, Rob Raiswell and an anonymous
788 reviewer, for their critical remarks, which significantly helped to improve this manuscript. All
789 geochemical data published in this paper are available under
790 http://dx.doi.org/10.1594/PANGAEA.832335.
791

792 **REFERENCES**

793 Algeo T. and Tribovillard N. (2009) Environmental analysis of paleoceanographic systems
794 based on molybdenum–uranium covariation. *Chem. Geol.* **268**, 211–225.

795 Aller R. C., Mackin J. and Cox R. (1986) Diagenesis of Fe and S in Amazon inner shelf
796 muds: apparent dominance of Fe reduction and implications for the genesis of
797 ironstones. *Cont. Shelf Res.* **6**, 263–289.

798 Anbar A. D., Creaser R., Papanastassiou D. and Wasserburg G. (1992) Rhenium in
799 seawater: Confirmation of generally conservative behavior. *Geochim. Cosmochim. Acta*
800 **56**, 4099–4103.

801 Arntz W. E., Brey T. and Gallardo A. (1994) Antarctic zoobenthos. *Oceanogr. Mar. Biol. An*
802 *Annu. Rev.* **32**, 241–304.

803 Babu C., Brumsack H.-J. and Schnetger B. (1999) Distribution of organic carbon in surface
804 sediments along the eastern Arabian Sea: a revisit. *Mar. Geol.* **162**, 91–103.

805 Barcena M. A., Gersonde R., Ledesma S., Fabres J., Calafat A. M., Canals M., Sierro F. J.,
806 Flores J. A., Bárcena M. A. and Fabrés J. (1998) Record of Holocene glacial oscillations
807 in Bransfield Basin as revealed by siliceous microfossil assemblages. *Antarct. Sci.* **10**,
808 269–285.

809 Barnes C. E. and Cochran J. K. (1990) Uranium removal in oceanic sediments and the
810 oceanic U balance. *Earth Planet. Sci. Lett.* **97**, 94–101.

811 Beck M., Dellwig O., Holstein J. M., Grunwald M., Liebezeit G., Schnetger B. and Brumsack
812 H.-J. (2008a) Sulphate, dissolved organic carbon, nutrients and terminal metabolic
813 products in deep pore waters of an intertidal flat. *Biogeochemistry* **89**, 221–238.

814 Beck M., Dellwig O., Schnetger B. and Brumsack H.-J. (2008b) Cycling of trace metals (Mn,
815 Fe, Mo, U, V, Cr) in deep pore waters of intertidal flat sediments. *Geochim. Cosmochim.*
816 *Acta* **72**, 2822–2840.

817 Benesch R. and Mangelsdorf P. (1972) Eine Methode zur colorimetrischen Bestimmung von
818 Ammoniak in Meerwasser. *Helgoländer Wissenschaftliche Meeresuntersuchungen* **23**,
819 365–375.

820 Bertine K. K. and Turekian K. K. (1973) Molybdenum in marine deposits. *Geochim.*
821 *Cosmochim. Acta* **37**, 1415–1434.

822 Bindschadler R., Choi H. and ASAID-Collaborators (2011) High-resolution image-derived
823 grounding and hydrostatic lines for the Antarctic Ice Sheet. Boulder, Colorado, USA:
824 National Snow and Ice Data Center. http://dx.doi.org/10.7265/N56T0JK2.

825 Boudreau B. (1997) *Diagenetic models and their impletation: modelling transport and*
826 *reactions in aquatic sediments*., Springer-Verlag, Berlin, Heidelberg, New York.

827 Boyd P. and Ellwood M. (2010) The biogeochemical cycle of iron in the ocean. *Nat. Geosci.*
828 **3**, 675–682.

829 Boyd P., Jickells T., Law C., Blain S., Boyle E., Buesseler K. O., Coale K. H., Cullen J., de
830 Baar H. J., Follows M., Harvey M., Lancelot C., Levasseur M., Owens N., Pollard R.,
831 Rivkin R., Sarmiento J., Schoemann V., Smetacek V., Takeda S., Tsuda A., Turner S.
832 and Watson A. (2007) Mesoscale iron enrichment experiments 1993-2005: Synthesis
833 and future directions. *Science* **315**, 612–617.

834 Brünjes R. M. (2013) The potentially bioavailable iron in melt waters and sediments of the
835 Potter Cove (King George Island, western Antarctic Peninsula). Master thesis, Carl-von-
836 Ossietzky Univ. Oldenburg.

837 Burdige D. J. (1993) The biogeochemistry of manganese and iron reduction in marine
838 sediments. *Earth-Science Rev.* **35**, 249–284.

839 Canfield D. E. (1989) Sulfate reduction and oxic respiration in marine sediments: implications
840 for organic carbon preservation in euxinic environments. *Deep Sea Res. Part A.*
841 *Oceanogr. Res. Pap.* **36**, 121–138.

842 Canfield D. E., Raiswell R. and Bottrell S. H. (1992) The reactivity of sedimentary iron
843 minerals toward sulfide. *Am. J. Sci.* **292**, 659–683.

844 Canfield D. E. and Thamdrup B. (2009) Towards a consistent classification scheme for
845 geochemical environments, or, why we wish the term “suboxic” would go away.
846 *Geobiology* **7**, 385–392.

847 Canfield D. E., Thamdrup B. and Hansen J. W. (1993) The anaerobic degradation of organic
848 matter in Danish coastal sediments: iron reduction, manganese reduction, and sulfate
849 reduction. *Geochim. Cosmochim. Acta* **57**, 3867–3883.

850 Chen M. and Wang W.-X. (2001) Bioavailability of natural colloid-bound iron to marine
851 plankton: Influences of colloidal size and aging. *Limnol. Oceanogr.* **46**, 1956–1967.

852 Church T., Sarin M., Fleisher M. and Ferdelman T. (1996) Salt marshes: An important
853 coastal sink for dissolved uranium. *Geochim. Cosmochim. Acta* **60**, 3879–3887.

854 Cline J. (1969) Spectrophotometric determination of hydrogen sulfide in natural waters.
855 *Limnol. Oceanogr.* **14**, 454–458.

856 Coale K. H., Johnson K. S., Chavez F. P., Buesseler K. O., Barber R. T., Brzezinski M. a,
857 Cochlan W. P., Millero F. J., Falkowski P. G., Bauer J. E., Wanninkhof R. H., Kudela R.
858 M., Altabet M. a, Hales B. E., Takahashi T., Landry M. R., Bidigare R. R., Wang X.,
859 Chase Z., Strutton P. G., Friederich G. E., Gorbunov M. Y., Lance V. P., Hilting A. K.,
860 Hiscock M. R., Demarest M., Hiscock W. T., Sullivan K. F., Tanner S. J., Gordon R. M.,
861 Hunter C. N., Elrod V. a, Fitzwater S. E., Jones J. L., Tozzi S., Koblizek M., Roberts A.
862 E., Herndon J., Brewster J., Ladizinsky N., Smith G., Cooper D., Timothy D., Brown S.
863 L., Selph K. E., Sheridan C. C., Twining B. S. and Johnson Z. I. (2004) Southern Ocean
864 iron enrichment experiment: carbon cycling in high- and low-Si waters. *Science* **304**,
865 408–14.

866 Colodner D., Edmond J. and Boyle E. (1995) Rhenium in the Black Sea: comparison with
867 molybdenum and uranium. *Earth Planet. Sci. Lett.* **131**, 1–15.

868 Colodner D., Sachs J., Ravizza G., Turekian K., Edmond J. and Boyle E. (1993) The
869 geochemical cycle of rhenium: a reconnaissance. *Earth Planet. Sci. Lett.* **117**, 205–221.

870 Crusius J., Calvert S., Pedersen T. and Sage D. (1996) Rhenium and molybdenum
871 enrichments in sediments as indicators of oxic, suboxic and anoxic conditions of
872 deposition. *Earth Planet. Sci. Lett.* **145**, 65–78.

873 Dellwig O., Beck M., Lemke A., Lunau M., Kolditz K., Schnetger B. and Brumsack H.-J.
874 (2007) Non-conservative behaviour of molybdenum in coastal waters: Coupling
875 geochemical, biological, and sedimentological processes. *Geochim. Cosmochim. Acta*
876 **71**, 2745–2761.

877 Dold B., Gonzales-Toril E., Aguilera A., Lopez-Pamo E., Cisternas M., Bucchi F. and Amils
878 R. (2013) Acid rock drainage and rock weathering in Antarctica: Important sources for
879 iron cycling in the Southern Ocean. *Environ. Sci. Technol.* **47**, 6129–6136.

880 Duff M., Coughlin J. and Hunter D. (2002) Uranium co-precipitation with iron oxide minerals.
881 *Geochim. Cosmochim. Acta* **66**, 3533–3547.

882 Dulaiova H., Ardelan M., Henderson P. and Charette M. A. (2009) Shelf-derived iron inputs
883 drive biological productivity in the southern Drake Passage. *Global Biogeochem. Cycles*
884 **23**, GB4014.

885 Dunbar R. B., Leventer A. R. and Stockton W. L. (1989) Biogenic sedimentation in McMurdo
886 Sound, Antarctica. *Mar. Geol.* **85**, 155–179.

887 Elderfield H., Mackenzie A., Berner R. A., Meadows P., Jones J., Clemmey H., Murchison D.,
888 Durand B., Eglinton G. and Sarnthein M. (1985) Element cycling in bottom sediments.
889 *Philos. Trans. R. Soc. B* **315**, 19–23.

890 Elrod V. A., Berelson W., Coale K. and Johnson K. (2004) The flux of iron from continental
891 shelf sediments: A missing source for global budgets. *Geophys. Res. Lett.* **31**, L12307.

892 Eraso A. and Dominguez M. del C. (2007) Physicochemical characteristics of the subglacier
893 discharge in potter cove, king george island, antarctica. In *Karst & Kryokarst, Studies of*
894 *the Faculty of Earth Sciences* (eds. A. Tyk and K. Stefaniak). University of Silesia. pp.
895 111–122.

896 Erickson B. E. and Helz G. R. (2000) Molybdenum(VI) speciation in sulfidic waters: Stability
897 and lability of thiomolybdates. *Geochim. Cosmochim. Acta* **64**, 1149–1158.

898 Franzmann P., Skyring G., Burton H. and Deprez P. (1988) Sulfate reduction rates and some
899 aspects of the limnology of four lakes and a fjord in the Vestfold Hills, Antarctica.
900 *Hydrobiologia* **165**, 25–33.

901 Froelich P., Klinkhammer G., Bender M., Luedtke N., Heath G., Cullen D., Dauphin P.,
902 Hammond D., Hartman B. and Maynard V. (1979) Early oxidation of organic matter in
903 pelagic sediments of the eastern Equatorial Atlantic - Suboxic diagenesis. *Geochim.*
904 *Cosmochim. Acta* **43**, 1075–1090.

905 Gribsholt B. and Kristensen E. (2003) Benthic metabolism and sulfur cycling along an
906 inundation gradient in a tidal spartina anglica salt marsh. *Limnol. Oceanogr.* **48**, 2151–
907 2162.

908 Hartnett H., Boehme S., Thomas C., DeMaster D. and Smith C. (2008) Benthic oxygen fluxes
909 and denitrification rates from high-resolution porewater profiles from the Western
910 Antarctic Peninsula continental shelf. *Deep Sea Res. Part II Top. Stud. Oceanogr.* **55**,
911 2415–2424.

912 Hatta M., Measures C. I., Selph K. E., Zhou M. and Hiscock W. T. (2013) Iron fluxes from the
913 shelf regions near the South Shetland Islands in the Drake Passage during the austral-
914 winter 2006. *Deep Sea Res. II* **90**, 89–101.

915 Helz G., Miller C., Charnock J., Mosselmans J., Pattrick R., Garner C. and Vaughan D. J.
916 (1996) Mechanism of molybdenum removal from the sea and its concentration in black
917 shales: EXAFS evidence. *Geochim. Cosmochim. Acta* **60**, 3631–3642.

Hopwood M. J., Statham P. J., Tranter M. and Wadham J. L. (2014) Glacial flours as a potential source of Fe(II) and Fe(III) to polar waters. *Biogeochemistry* **118**, 443–452.

Howarth R. and Jørgensen B. B. (1984) Formation of 35S-labelled elemental sulfur and pyrite in coastal marine sediments (Limfjorden and Kysing Fjord, Denmark) during short-term 35SO42− reduction measurements. *Geochim. Cosmochim. Acta* **48**, 1807–1818.

Iken K., Quartino M., Barrera-Oro E., Palermo J., Wiencke C. and Brey T. (1998) Trophic relations between macroalgae and herbivores. In *The Potter Cove coastal ecosystem, Antarctica. Berichte zur Polarforschung 299* (eds. C. Wiencke, G. Ferreyra, W. Arntz, and C. Rinaldi). pp. 258–262.

Jakobsen R. and Postma D. (1989) Formation and solid-solution behaviour of Ca-rhodochrosites in marine muds of the Baltic Deeps. *Geochim. Cosmochim. Acta* **53**, 2639–2648.

Jiang M., Barbeau K. A., Selph K. E., Measures C. I., Buck K. N., Azam F., Mitchell B. G. and Zhou M. (2013) The role of organic ligands in iron cycling and primary productivity in the Antarctic Peninsula: A modeling study. *Deep Sea Res. II* **90**, 112–133.

De Jong J., Schoemann V., Lannuzel D., Croot P., de Baar H. J. and Tison J.-L. (2012) Natural iron fertilization of the Atlantic sector of the Southern Ocean by continental shelf sources of the Antarctic Peninsula. *J. Geophys. Res.* **117**, G01029.

Jørgensen B. B. (1982) Mineralization of organic matter in the sea bed - the role of sulphate reduction. *Nature* **296**, 643–645.

Kattner G. (1999) Storage of dissolved inorganic nutrients in seawater: poisoning with mercury chloride. *Mar. Chem.* **67**, 61–66.

Khim B.-K. K. and Yoon H. Il (2003) Postglacial marine environmental changes in Maxwell Bay, King George Island, West Antarctica. *Polar Res.* **22**, 341–353.

King S., Froelich P. N. and Jahnke R. (2000) Early diagenesis of germanium in sediments of the Antarctic South Atlantic: In search of the missing Ge sink. *Geochim. Cosmochim. Acta* **64**, 1375–1390.

Klinkhammer G. and Palmer M. (1991) Uranium in the oceans: where it goes and why. *Geochim. Cosmochim. Acta* **55**, 1799–1806.

947 Klöser H., Ferreyra G., Schloss I. R., Mercuri G., Laturnus F. and Curtosi A. (1994)
948 Hydrography of Potter Cove, a small fjord-like inlet on King George Island (South
949 Shetlands). *Estuar. Coast. Shelf Sci.* **38**, 523–537.

950 Kostka J. E., Thamdrup B., Glud R. N. and Canfield D. E. (1999) Rates and pathways of
951 carbon oxidation in permanently cold Arctic sediments. *Mar. Ecol. Prog. Ser.* **180**, 7–21.

952 Ku T.-L., Knauss K. G. and Mathieu G. G. (1977) Uranium in open ocean: concentration and
953 isotopic composition. *Deep Sea Res.* **24**, 1005–1017.

954 Lam P. J. and Bishop J. K. (2008) The continental margin is a key source of iron to the HNLC
955 North Pacific Ocean. *Geophys. Res. Lett.* **35**, L07608.

956 Lam P. J., Ohnemus D. C. and Marcus M. A. (2012) The speciation of marine particulate iron
957 adjacent to active and passive continental margins. *Geochim. Cosmochim. Acta* **80**,
958 108–124.

959 Lancelot C., De Montety A., Goosse H., Becquevort S., Schoemann V., Pasquer B. and
960 Vancoppenolle M. (2009) Spatial distribution of the iron supply to phytoplankton in the
961 Southern Ocean: a model study. *Biogeosciences* **6**, 2861–2878.

962 Langmuir D. (1978) Uranium solution-mineral equilibria at low temperatures with applications
963 to sedimentary ore deposits. *Geochim. Cosmochim. Acta* **42**, 547–569.

964 Lee Y. Il, Lim H. S., Yoon H. Il and Lee I. Y. (2009) Carbon and nitrogen isotope composition
965 of vegetation on King George Island, maritime Antarctic. *Polar Biol.* **32**, 1607–1615.

966 Lettmann K. A., Riedinger N., Ramlau R., Knab N., Böttcher M. E., Khalili A., Wolff J.-O. and
967 Jørgensen B. B. (2012) Estimation of biogeochemical rates from concentration profiles:
968 A novel inverse method. *Estuar. Coast. Shelf Sci.* **100**, 26–37.

969 Lim C. H. (2014) Modelling waves and currents in Potter Cove, King George Island,
970 Antarctica. Ph. D. thesis, Carl-von-Ossietzky Univ. Oldenburg.

971 Lovley D. R., Phillips E. J., Gorby Y. A. and Landa E. R. (1991) Microbial reduction of
972 uranium. *Nature* **350**, 413–416.

973 Madison A., Tebo B., Mucci A., Sundby B. and Luther III G. W. (2013) Abundant porewater
974 Mn(III) is a major component of the sedimentary redox system. *Science* **341**, 875–878.

975 Majewski W., Wellner J. S., Szczuciński W. and Anderson J. B. (2012) Holocene
976 oceanographic and glacial changes recorded in Maxwell Bay, West Antarctica. *Mar.*
977 *Geol.* **326-328**, 67–79.

978 Martin J. H., Gordon R. M. and Fitzwater S. E. (1990) Iron in Antarctic waters. *Nature* **345**,
979 156–158.

980 Measures C. I., Brown M., Selph K. E., Apprill A., Zhou M., Hatta M. and Hiscock W. T.
981 (2013) The influence of shelf processes in delivering dissolved iron to the HNLC waters
982 of the Drake Passage, Antarctica. *Deep Sea Res. II* **90**, 77–88.

983 Measures C. I., Hatta M. and Grand M. M. (2012) Bioactive trace metal distributions and
984 biogeochemical controls in the Southern Ocean. *Oceanography* **25**, 122–133.

985 Middleburg J. J., de Lange G. J. and Vanderweijden C. H. (1987) Manganese solubility
986 control in marine pore waters. *Geochim. Cosmochim. Acta* **51**, 759–763.

987 Milliken K. T., Anderson J. B., Wellner J. S., Bohaty S. M. and Manley P. L. (2009) High-
988 resolution Holocene climate record from Maxwell Bay, South Shetland Islands,
989 Antarctica. *Geol. Soc. Am. Bull.* **121**, 1711–1725.

990 Miranda K., Espey M. and Wink D. (2001) A rapid, simple spectrophotometric method for
991 simultaneous detection of nitrate and nitrite. *Nitric Oxide* **5**, 62–71.

992 Monien P., Schnetger B., Brumsack H.-J., Hass H. C. and Kuhn G. (2011) A geochemical
993 record of late Holocene palaeoenvironmental changes at King George Island (maritime
994 Antarctica). *Antarct. Sci.* **23**, 255–267.

995 Morford J. L., Emerson S. R., Breckel E. J. and Kim S. H. (2005) Diagenesis of oxyanions (V,
996 U, Re, and Mo) in pore waters and sediments from a continental margin. *Geochim.*
997 *Cosmochim. Acta* **69**, 5021–5032.

998 Morford J. L., Martin W. R. and Carney C. M. (2012) Rhenium geochemical cycling: Insights
999 from continental margins. *Chem. Geol.* **324-325**, 73–86.

1000 Morford J. L., Martin W. R., François R. and Carney C. M. (2009) A model for uranium,
1001 rhenium, and molybdenum diagenesis in marine sediments based on results from
1002 coastal locations. *Geochim. Cosmochim. Acta* **73**, 2938–2960.

1003 Morford J. L., Martin W. R., Kalnejais L. H., François R., Bothner M. and Karle I.-M. (2007)
1004 Insights on geochemical cycling of U, Re and Mo from seasonal sampling in Boston
1005 Harbor, Massachusetts, USA. *Geochim. Cosmochim. Acta* **71**, 895–917.

1006 Morris A. (1975) Dissolved molybdenum and vanadium in the northeast Atlantic Ocean.
1007 *Deep Sea Res. Oceanogr. Abstr.* **22**, 49–54.

1008 Mucci A. (2004) The behavior of mixed Ca-Mn carbonates in water and seawater: Controls of
1009 manganese concentrations in marine porewaters. *Aquat. Geochemistry* **10**, 139–169.

1010 Nedwell D. (1989) Benthic microbial activity in an Antarctic coastal sediment at Signy Island,
1011 South Orkney Islands. *Estuar. Coast. Shelf Sci.* **28**, 507–516.

1012 Nedwell D. and Walker T. R. (1995) Sediment-water fluxes of nutrients in an Antarctic
1013 coastal environment: influence of bioturbation. *Polar Biol.* **15**, 57–64.

1014 Pasotti F., Manini E., Giovannelli D., Wölfl A.-C., Monien D., Verleyen E., Braeckman U.,
1015 Abele D. and Vanreusel A. (accepted manuscript) Antarctic shallow water benthos
1016 under glacier retreat forcing. *Mar. Ecol.*

1017 Planquette H., Statham P. J., Fones G. R., Charette M. A., Moore C. M., Salter I., Nédélec F.
1018 H., Taylor S. L., French M., Baker A., Mahowald N. and Jickells T. (2007) Dissolved iron
1019 in the vicinity of the Crozet Islands, Southern Ocean. *Deep Sea Res. II* **54**, 1999–2019.

1020 Postma D. (1993) The reactivity of iron oxides in sediments: A kinetic approach. *Geochim.*
1021 *Cosmochim. Acta* **57**, 5027–5034.

1022 Poulton S. W., Krom M. D. and Raiswell R. (2004) A revised scheme for the reactivity of
1023 iron(oxyhydr)oxide minerals towards dissolved sulfide. *Geochim. Cosmochim. Acta* **68**,
1024 3703–3715.

1025 Poulton S. W. and Raiswell R. (2005) Chemical and physical characteristics of iron oxides in
1026 riverine and glacial meltwater sediments. *Chem. Geol.* **218**, 203–221.

1027 Quartino M. L., Deregibus D., Campana G. L., Latorre G. E. J. and Momo F. R. (2013)
1028 Evidence of macroalgal colonization on newly ice-free areas following glacial retreat in
1029 Potter Cove (South Shetland Islands), Antarctica. *PLoS One* **8**, e58223.

1030 Quartino M. L. and de Zaixso A. L. B. (2008) Summer macroalgal biomass in Potter Cove,
1031 South Shetland Islands, Antarctica: Its production and flux to the ecosystem. *Polar Biol.*
1032 **31**, 281–294.

1033 Raiswell R. (2011) Iceberg-hosted nanoparticulate Fe in the Southern Ocean: Mineralogy,
1034 origin, dissolution kinetics and source of bioavailable Fe. *Deep Sea Res. II* **58**, 1364–
1035 1375.

1036 Raiswell R. and Anderson T. (2005) Reactive iron enrichment in sediments deposited
1037 beneath euxinic bottom waters: constraints on supply by shelf recycling. *Geol. Soc.*
1038 *London, Spec. Publ.* **248**, 179–194.

1039 Raiswell R., Benning L., Tranter M. and Tulaczyk S. (2008) Bioavailable iron in the Southern
1040 Ocean: The significance of the iceberg conveyor belt. *Geochem. Trans.* **9**.

1041 Raiswell R. and Canfield D. E. (1996) Rates of reaction between silicate iron and dissolved
1042 sulfide in Peru Margin sediments. *Geochim. Cosmochim. Acta* **60**, 2777–2787.

1043 Raiswell R. and Canfield D. E. (1998) Sources of iron for pyrite formation in marine
1044 sediments. *Am. J. Sci.* **298**, 219–245.

1045 Raiswell R. and Canfield D. E. (2012) The iron biogeochemical cycle past and present.
1046 *Geochemical Perspect.* **1**, 1–220.

1047 Raiswell R., Tranter M., Benning L., Siegert M., De'ath R., Huybrechts P. and Payne T.
1048 (2006) Contributions from glacially derived sediment to the global iron (oxyhydr)oxide
1049 cycle: implications for iron delivery to the oceans. *Geochim. Cosmochim. Acta* **70**,
1050 2765–2780.

1051 Redfield A. C., Ketchum B. H. and Richards F. A. (1963) The influence of organisms on the
1052 composition of sea-water. In *The Sea: Ideas and observations on progress in the study*
1053 *of the seas* (ed. N. M. Hill). Interscience Publishers, New York. pp. 26–77.

1054 Rodushkin I. (1998) Capabilities of high resolution inductively coupled plasma mass
1055 spectrometry for trace element determination in plant sample digests. *Fresenius J. Anal.*
1056 *Chem.* **362**, 541–546.

1057 Roese M. and Drabble M. (1998) Wind driven circulation in Potter Cove. In *The Potter Cove*
1058 *coastal ecosystem, Antarctica* (eds. C. Wiencke, G. A. Ferreyra, W. Arntz, and C.
1059 Rinaldi). *Rep. Polar Res.*, **299**. 40–46.

Rückamp M., Braun M., Suckro S. and Blindow N. (2011) Surface lowering , accumulation and area changes of the King George Island ice cap , Antarctica. *Glob. Planet. Change* **79**, 99–109.

Rue E. L. and Bruland K. W. (1995) Complexation of iron(III) by natural organic ligands in the Central North Pacific as determined by a new competitive ligand equilibration/adsorptive cathodic stripping voltammetric method. *Mar. Chem.* **50**, 117–138.

Rysgaard S., Finster K. and Dahlgaard H. (1996) Primary production, nutrient dynamics and mineralisation in a northeastern Greenland fjord during the summer thaw. *Polar Biol.* **16**, 497–506.

Rysgaard S., Thamdrup B., Risgaard-Petersen N., Fossing H., Berg P., Christensen P. B. and Dalsgaard T. (1998) Seasonal carbon and nutrient mineralization in a high-Arctic coastal marine sediment, Young Sound, Northeast Greenland. *Mar. Ecol. Prog. Ser.* **175**, 261–276.

Sani R., Peyton B., Amonette J. and Geesey G. (2004) Reduction of uranium(VI) under sulfate-reducing conditions in the presence of Fe(III)-(hydr)oxides. *Geochim. Cosmochim. Acta* **68**, 2639–2648.

Sarazin G., Michard G. and Prevot F. (1999) A rapid and accurate spectroscopic method for alkalinity measurements in sea water samples. *Water Res.* **33**, 290–294.

Schloss I. R., Abele D., Moreau S., Demers S., Bers A. V., González O. and Ferreyra G. A. (2012) Resonse of phytoplankton dynamics to 19-year (1991-2009) climate trends in Potter Cove (Antarctica). *J. Mar. Syst.* **92**, 53–66.

Schloss I. R., Ferreyra G. A. and Ruiz-Pino D. (2002) Phytoplankton biomass in Antarctic shelf zones: a conceptual model based on Potter Cove, King George Island. *J. Mar. Syst.* **36**, 129–143.

Schnetger B. and Lehners C. (2014) Determination of nitrate plus nitrite in small volume marine water samples using vanadium(III)chloride as a reduction agent. *Mar. Chem.* **160**, 91–98.

Scholz F., Hensen C., Noffke A., Rohde A., Liebetrau V. and Wallmann K. (2011) Early diagenesis of redox-sensitice trace metals in the Peru upwelling area - response to ENSO-related oxygen fluctuations in the water column. *Geochim. Cosmochim. Acta* **75**, 7257–7276.

1091 Schroth A. W., Crusius J., Sholkovitz E. R. and Bostick B. C. (2009) Iron solubility driven by
1092 speciation in dust sources to the ocean. *Nat. Geosci.* **2**, 337–340.

1093 Shaw T. J., Gieskes J. M. and Jahnke R. A. (1990) Early diagenesis in differing depositional
1094 environments: The response of transition metals in pore water. *Geochim. Cosmochim.*
1095 *Acta* **54**, 1233–1246.

1096 Shaw T. J., Raiswell R., Hexel C., Vu H., Moore W. S., Dudgeon R. and Smith K. L. (2011)
1097 Input, composition, and potential impact of terrigenous material from free-drifting
1098 icebergs in the Weddell Sea. *Deep Sea Res. Part II Top. Stud. Oceanogr.* **58**, 1376–
1099 1383.

1100 Sholkovitz E. (1973) Interstitial water chemistry of the Santa Barbara Basin sediments.
1101 *Geochim. Cosmochim. Acta* **37**, 2043–2073.

1102 Skoog D. A. and Leary J. J. (1996) *Instrumentelle Analytik*., Springer, Berlin.

1103 Sørensen J., Jørgensen B. B. and Revsbech N. P. (1979) A comparison of oxygen, nitrate,
1104 and sulfate respiration in coastal marine sediments. *Microb. Ecol.* **5**, 105–115.

1105 Stumm W. and Morgan J. J. (1981) *Aquatic Chemistry, 2nd Edition*. 2nd ed., Wiley-
1106 Interscience, New York.

1107 Tagliabue A., Bopp L., Dutay J.-C., Bowie A. R., Chever F., Jean-Baptiste P., Bucciarelli E.,
1108 Lannuzel D., Remenyi T., Sarthou G., Aumont O., Gehlen M. and Jeandel C. (2010)
1109 Hydrothermal contribution to the oceanic dissolved iron inventory. *Nat. Geosci.* **3**, 252–
1110 256.

1111 Takahashi T., Williams R. and Bos D. (1982) Carbonate chemistry. In *GEOSECS Pacific*
1112 *Expedition, Volume 3: Hydrographic Data 1973-1974* (eds. W. S. Broecker, D. W.
1113 Spencer, and H. Craig). National Science Foundation, Washington D.C. pp. 77–83.

1114 Thamdrup B. and Canfield D. E. (1996) Pathways of carbon oxidation in continental margin
1115 sediments off central Chile. *Limnol. Oceanogr.* **41**, 1629–1650.

1116 Timmermann R., Le Brocq A., Deen T., Domack E. W., Dutrieux P., Galton-Fenzi B., Hellmer
1117 H., Humbert A., Jansen D., Jenkins A., Lambrecht A., Makinson K., Niederjasper F.,
1118 Nitsche F., Nøst O., Smedsrud L. and Smith W. (2010) A consistent data set of Antarctic
1119 ice sheet topography, cavity geometry, and global bathymetry. *Earth Syst. Sci. Data* **2**,
1120 261–273.

Tribovillard N., Algeo T. J., Lyons T. and Riboulleau A. (2006) Trace metals as paleoredox and paleoproductivity proxies: An update. *Chem. Geol.* **232**, 12–32.

Tribovillard N., Riboulleau A., Lyons T. and Baudin F. (2004) Enhanced trapping of molybdenum by sulfurized marine organic matter of marine origin in Mesozoic limestones and shales. *Chem. Geol.* **213**, 385–401.

Tromp T., van Cappellen P. and Key R. (1995) A global model for the early diagenesis of organic carbon and organic phosphorus in marine sediments. *Geochim. Cosmochim. Acta* **59**, 1259–1284.

Trouwborst R. E., Clement B. G., Tebo B. M., Glazer B. T. and Luther III G. W. (2006) Soluble Mn(III) in suboxic zones. *Science* **313**, 1955–1957.

Vandieken V., Nickel M. and Jørgensen B. B. (2006) Carbon mineralization in Arctic sediments northeast of Svalbard: Mn(IV) and Fe(III) reduction as principal anaerobic respiratory pathways. *Mar. Ecol. Prog. Ser.* **322**, 15–27.

Vorlicek T. P., Kahn M. D., Kasuya Y. and Helz G. R. (2004) Capture of molybdenum in pyrite-forming sediments: Role of ligand-induced reduction by polysulfides. *Geochim. Cosmochim. Acta* **68**, 547–556.

Wadham J., De'ath R., Monteiro F., Tranter M., Ridgwell A., Raiswell R. and Tulaczyk S. (2013) The potential role of the Antarctic Ice Sheet in global biogeochemical cycles. *Earth Environ. Sci. Trans. R. Soc. Edinburgh* **104**, 55–67.

Weston N. B., Porubsky W. P., Samarkin V. A., Erickson M., Macavoy S. E. and Joye S. B. (2006) Porewater stoichiometry of terminal metabolic products, sulfate, and dissolved organic carbon and nitrogen in estuarine intertidal creek-bank sediments. *Biogeochemistry* **77**, 375–408.

Weykam G., Gómez C., Wiencke C., Iken K. and Klöser H. (1996) Photosynthetic characteristics and C:N ratios of macroalgae from King George Island (Antarctica). *J. Exp. Mar. Bio. Ecol.* **204**, 1–22.

Yoon H. Il, Yoo K.-C., Park B.-K., Kim Y., Khim B.-K. and Kang C.-Y. (2004) The origin of massive diamicton in Marian and Potter coves, King George Island, West Antarctica. *Geosci. J.* **8**, 1–10.

Zheng Y., Anderson R. F., van Geen A. and Kuwabara J. (2000) Authigenic molybdenum formation in marine sediments: a link to pore water sulfide in the Santa Barbara Basin. *Geochim. Cosmochim. Acta* **64**, 4165–4178.

Zhou M., Zhu Y., Measures C. I., Hatta M., Charette M. A., Gille S. T., Frants M., Jiang M. and Mitchell B. G. (2013) Winter mesoscale circulation on the shelf slope region of the southern Drake Passage. *Deep Sea Res. II* **90**, 4–14.

Figures and Tables

Fig. 1. Map of the study site with sampling locations. Sediment cores (squares) and surface samples (grey dots) were taken during austral summers 2009/2010 and 2010/2011. Black squares mark sediment cores where pore water data are available.

Fig. 2. Pore water profiles of nutrients (NO_3^-, NH_4^+, PO_4^{3-}), redox-sensitive trace metals (Fe, Mn, Mo, U, Re), sulphate depletion ($SO_4^{2-}{}_{dep}$), H_2S, and total alkalinity (TA) from core P04 close to the tidewater glacier front.

Fig. 3. Pore water profiles of nutrients (NO_3^-, NH_4^+, PO_4^{3-}), redox-sensitive trace metals (Fe, Mn, Mo, U, Re), sulphate depletion ($SO_4^{2-}{}_{dep}$), H_2S, and total alkalinity (TA) from cores P05 (black dot) and P08 (white triangle) obtained from the central Potter Cove.

Fig. 4. Pore water profiles of nutrients (NO_3^-, NH_4^+, PO_4^{3-}), redox-sensitive trace metals (Fe, Mn, Mo, U, Re), sulphate depletion ($SO_4^{2-}{}_{dep}$), H_2S, and total alkalinity (TA) from cores P07 (black dot) and K48 (white triangle) obtained

close to the southern coast of Potter Peninsula. Note that no NH_4^+ and H_2S data is available for core K48.

Fig. 5. Ratios of total alkalinity (TA) to sulphate depletion ($SO_4^{2-}{}_{dep}$) in pore waters from Potter Cove sediments with best-fit linear regressions.

Fig. 6. a) Pore water profiles of sulphate (SO_4^{2-}) and b) modelled sulphate reduction rates (SRR) for the upper 20 cm of cores P07, KX4, K23, and K48 using the REC model after Lettmann et al. (2012) and a smoothing parameter λ of 10. For more information about λ see Lettmann et al. (2012).

Fig. 7. Contourplots of several pore water (Fe, Mn, $SO_4^{2-}{}_{dep}$, PO_4^{3-}, TA) and solid phase parameters (TOC, TS) of Potter Cove sediments.

Table 1. Overview of pore water core locations, including sampling date, UTM coordinates (Zone Z21E; WGS84), water depth, coring gear and core length (recovery in brackets). GC: gravity corer, PC: push corer.

Table 2. Precision and accuracy of pore water (Fe, Mn, Mo, Na, Re, U, PO_4^{3-}, NO_x^-, NO_2^-, NH_4^+, SO_4^{2-}) and solid phase (TS, TC, TIC) analyses of Potter Cove sediments. Precision is given as relative standard deviation (RSD%). In case of TOC and NO_3^- accuracy and precision represent the relative maximum errors.

Table 3. Total fluxes of dissolved iron derived from selected Potter Cove sediments estimated by using the REC model after Lettmann et al. (2012) and a smoothing parameter λ of 10. For more information about λ see Lettmann et al. (2012).

Table 4. Compilation of inputs and fluxes of bioavailable iron (Fe_b) to the Southern Ocean from different sources. Data are from [a] this study, [b] Lancelot et al. (2009), [c] Tagliabue et al. (2010), [d] Dulaiova et al. (2009), [e] Dold et al. (2013), [f] Raiswell and Canfield (2012), [g], Shaw et al. (2011), and [h] Wadham et al. (2013). Export efficiencies are 5% for shelf-derived fluxes (*) and 1% for subglacial meltwaters ($^+$). Note that the shelf-derived Fe flux given by Dulaiova et al. (2009) is based on an area of 250 x 250 km.

Table 1 - Core locations

Core name	Sampling Date	Grid	Easting	Northing	Water Depth (m)	Gear	Core length (cm)
PC/P01	28/12/2011	21E	414712	3099674	~30	GC	29.0
PC/P02	17/01/2011	21E	414796	3099363	9.7	GC	45.0 (44.0)
PC/P03	04/02/2011	21E	414146	3099280	32	GC	45.0 (44.0)
PC/P04	04/02/2011	21E	414593	3099976	43	GC	43.0
PC/P05	08/01/2011	21E	413518	3099007	36	GC	30.0 (28.0)
PC/P06	20/01/2011	21E	413473	3099270	37	GC	27.0
PC/P07	20/01/2011	21E	413256	3098391	4.7	GC	26.0
PC/P08	01/02/2011	21E	413100	3099000	42	GC	37.0
PC/K17	11/02/2010	21E	413075	3098606	23	GC	27.0 (25.0)
PC/K23	28/01/2010	21E	412888	3098794	29	GC	29.0
PC/K48	01/03/2010	21E	413906	3098827	12	PC	17.5 (16.0)
PC/KX1	03/02/2010	21E	413304	3098560	21	PC	18.5 (18.0)
PC/KX4	18/02/2010	21E	414493	3099121	10	PC	27.0 (24.0)

Table 2 - Accuracy and precision of methods

	Precision (%)	Accuracy (%)
NO_x^-	5.0	2.0
NO_2^-	4.2	-2.6
NO_3^-	6.0	2.5
NH_4^+	2.9	1.3
TA	2.8	0.03
Na	1.4	5.7
PO_4^{3-}	1.0	0.2
SO_4^{2-}	1.4	-5.3
Mn	4.1	-2.0
Fe	3.0	-2.0
Mo	1.7	0.1
Re	7.5	-11.2
U	2.1	-1.7
TS	5.0	2.5
TC	1.2	-0.6
TIC	1.0	0.5
TOC	2.4	-0.8

Table 3 - Iron fluxes of Potter Cove

Core	Total iron flux (mmol m^{-2} yr^{-1})
P01	15
P02	4
P04	14
P05	155
P08	114
KX4	1

Table 4 - Compilation of iron fluxes to the Southern Ocean

Source	Input Fe_b (x 10^3 t yr^{-1})	Flux Fe_b Southern Ocean (mg m^{-2} yr^{-1})
Shelf sediments	6.9–790*	0.35–39.5 [a]
	1.05*	0.05 [b]
	13–32*	0.64–1.6 [c]
	2.3	37 [d]
Acid rock drainage	1	0.00005 [e]
Dust	4.1–20	0.21–1 [f]
		0.05–0.25 [g]
	0.8	0.04 [b]
Icebergs	750–1250	37.5–62.5 [f]
	40–400	2–20 [g]
Subglacial meltwater (anoxic)	0.11–110+	0.0055–5.5 [h]

Fig. 1 - Map of study site

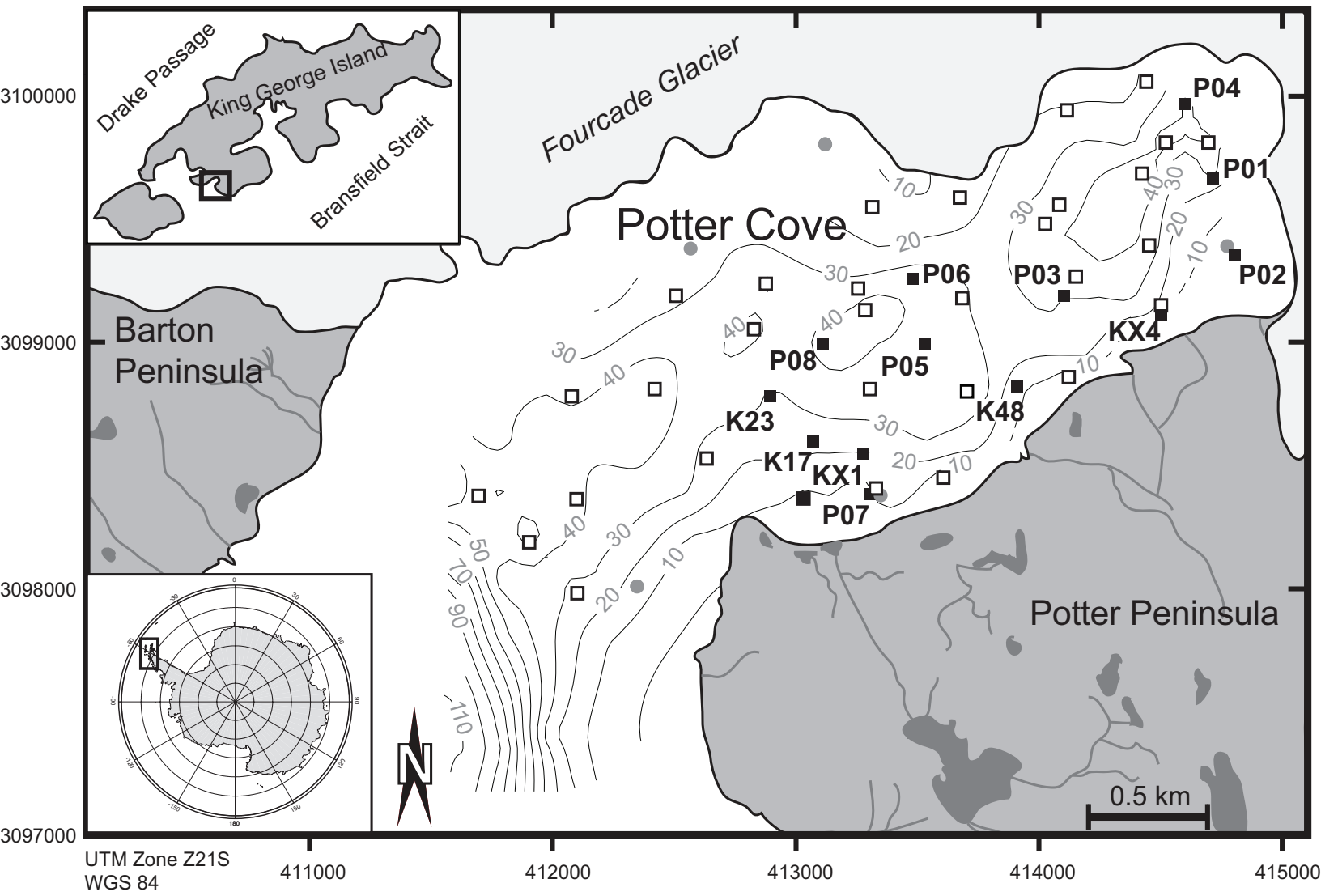

Fig. 2 - Pore water profiles core P04

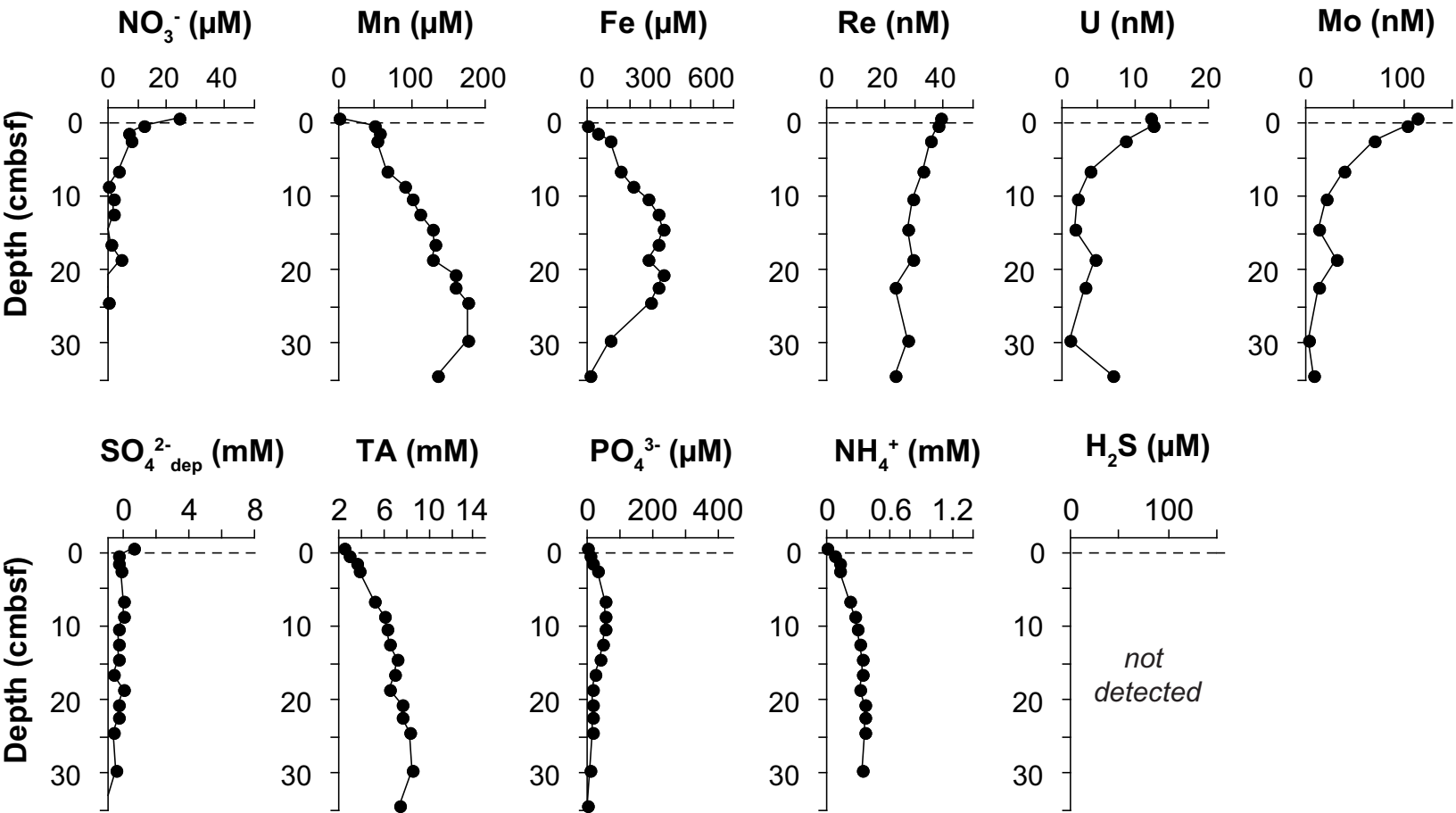

Fig. 3 - Pore water profiles core P05 & P08

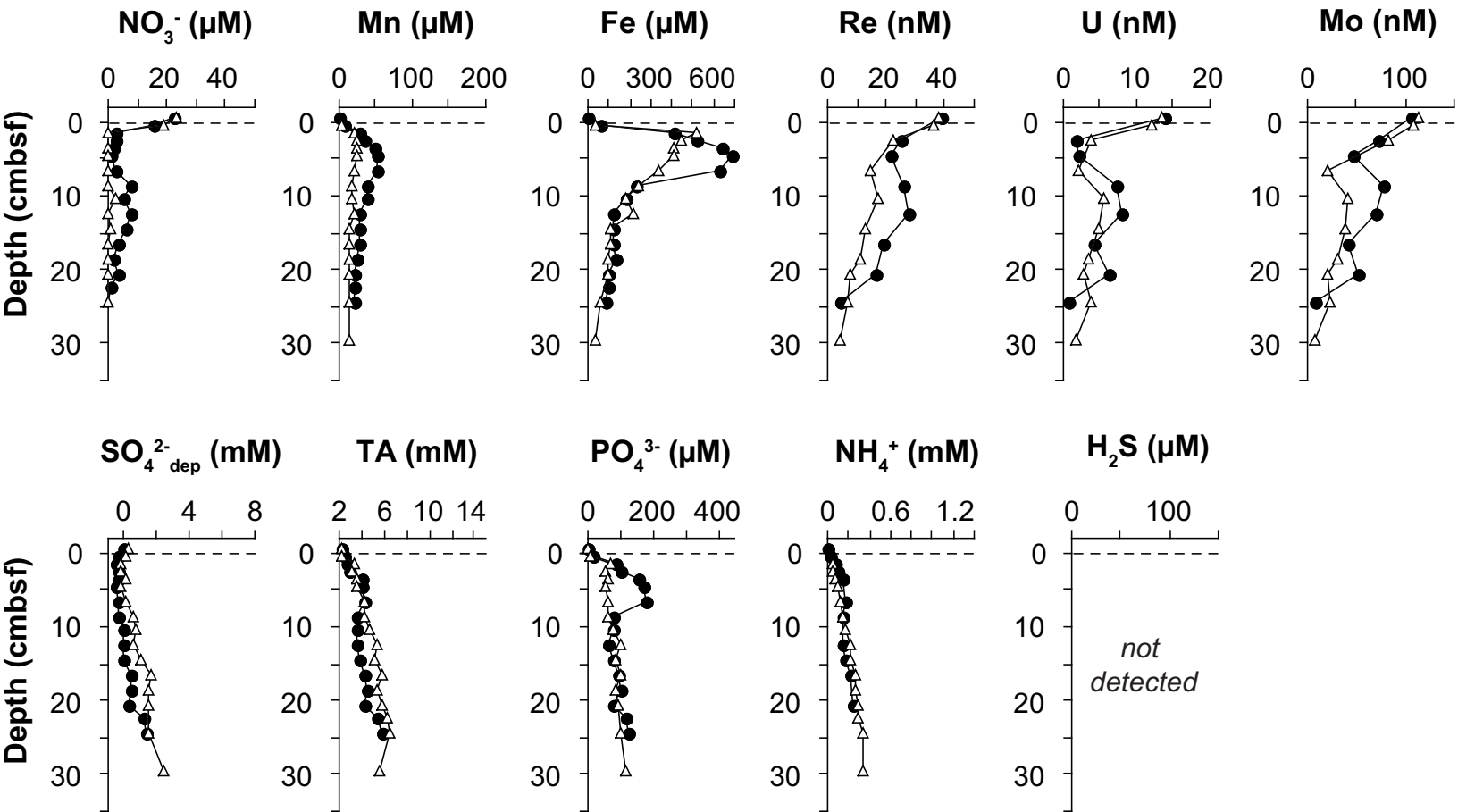

Fig. 4 - Pore water profiles core P07 & K48

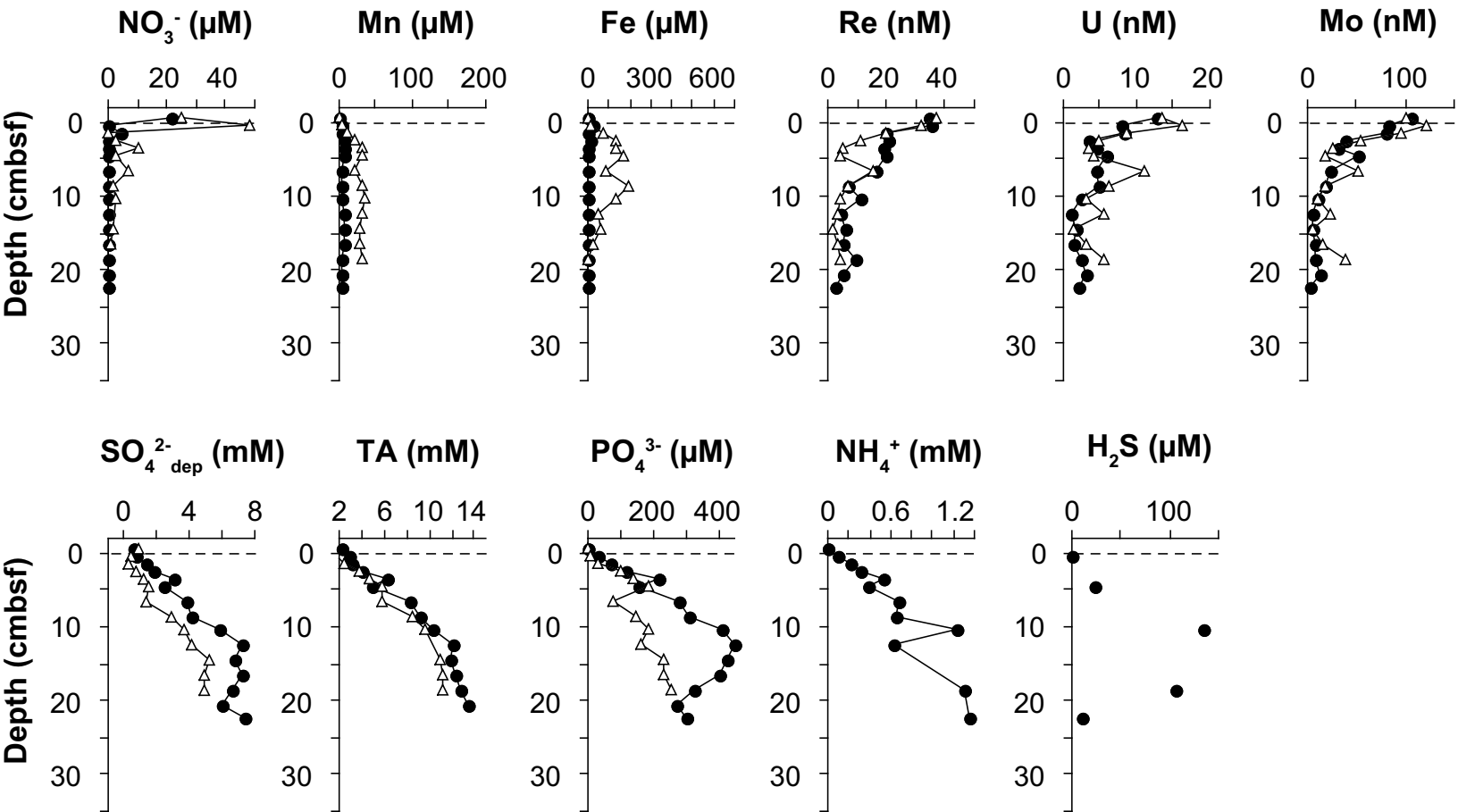

Fig. 5 - Sulphate depletion vs total alkalinity

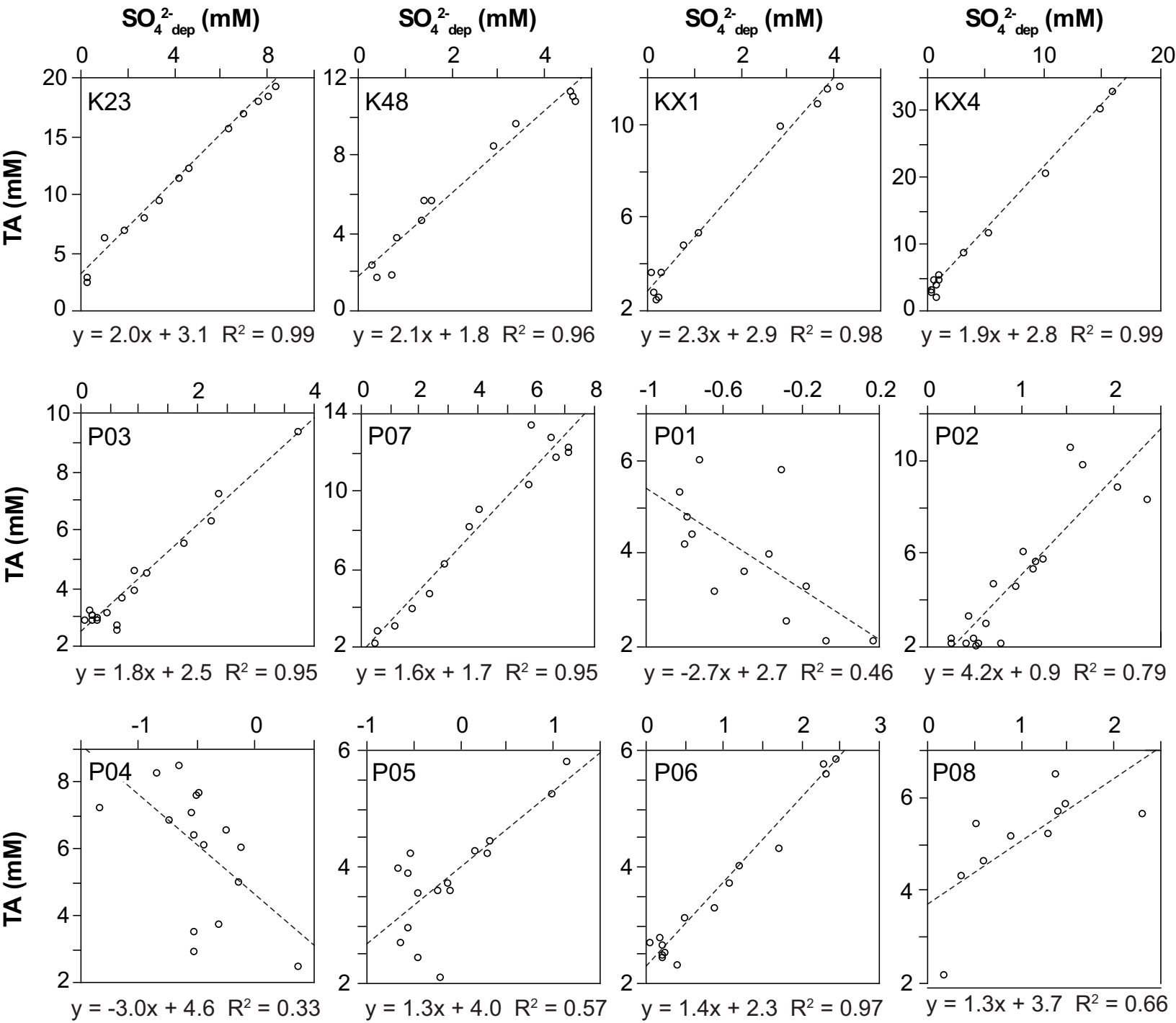

Fig. 6 - Sulphate reduction rates

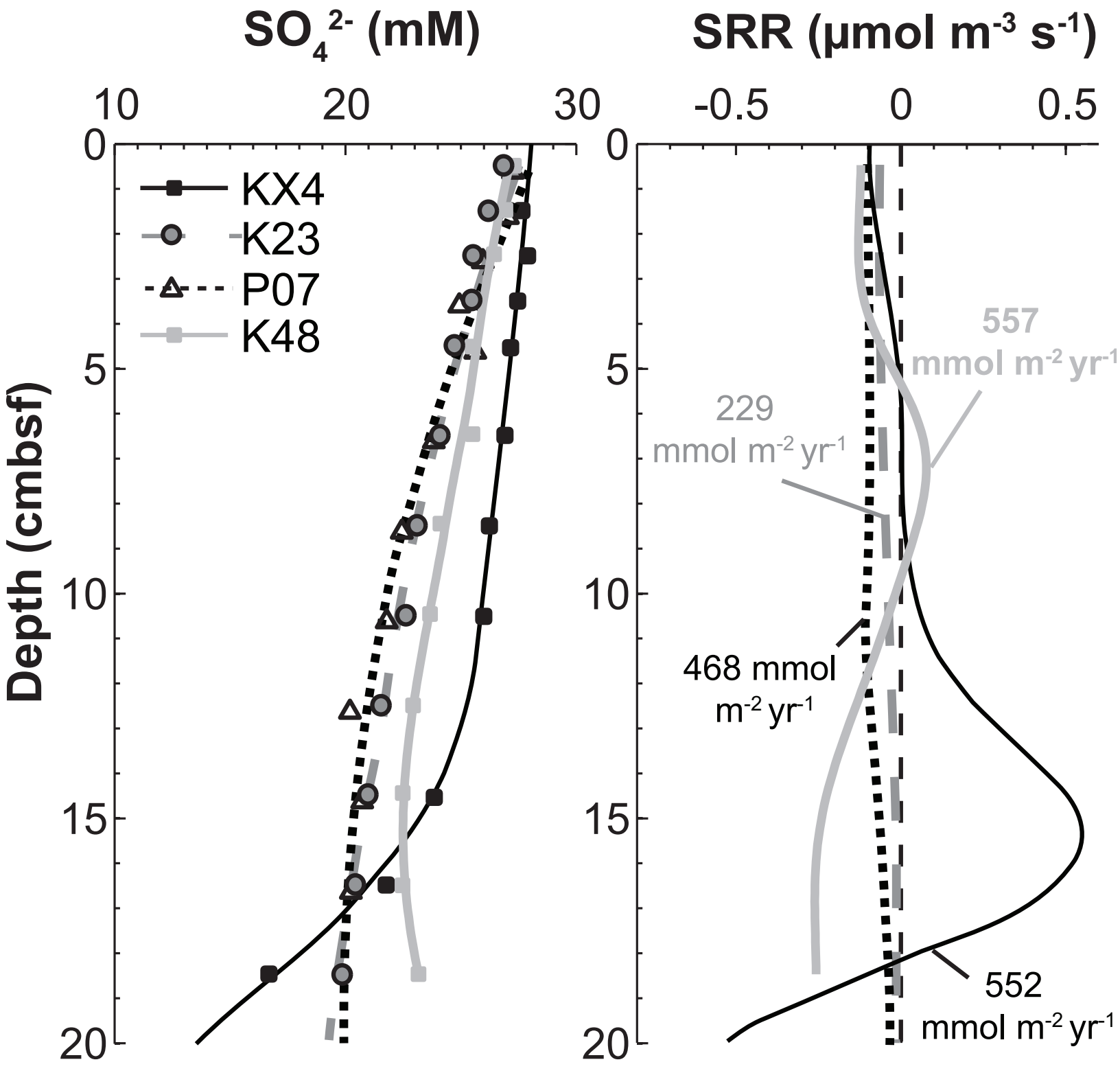

Fig. 7 - Spatial distribution of pore water and bulk parameters

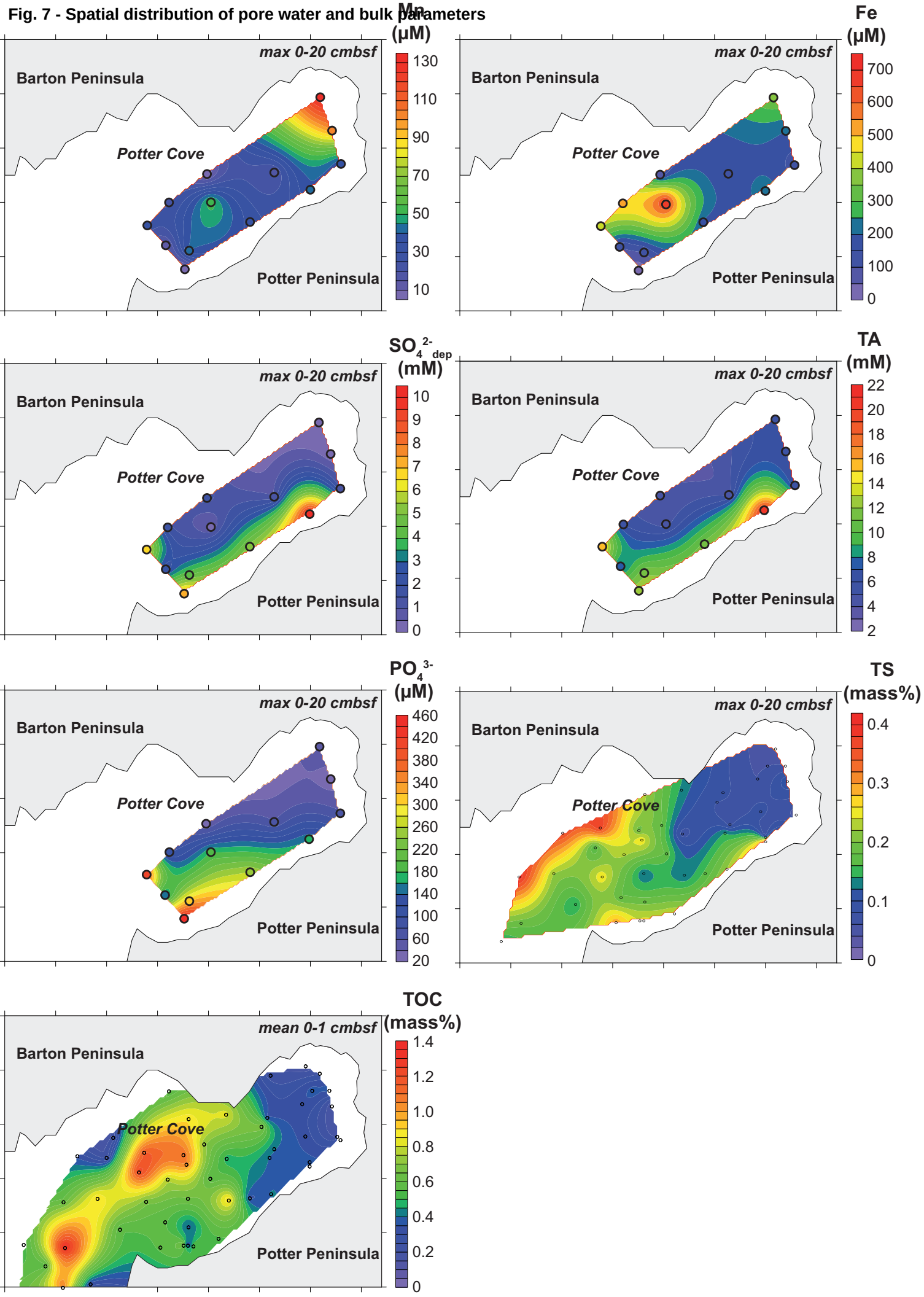

Revised Manuscript (Track Changes Mode)

Click here to download Electronic Annex: Monien et al. revised (Track Changes Mode).pdf